Metabolism 139 (2023) 155372

Contents lists available at ScienceDirect

Metabolism

journal homepage: www.journals.elsevier.com/metabolism

FAM3A maintains metabolic homeostasis by interacting with F1-ATP synthase to regulate the activity and assembly of ATP synthase

Han Yan [a,1], Yuhong Meng [a,1], Xin Li [a,1], Rui Xiang [a], Song Hou [a], Junpei Wang [a], Lin Wang [b], Xiaoxing Yu [a], Ming Xu [c], Yujing Chi [d,*], Jichun Yang [a,*]

[a] Department of Physiology and Pathophysiology, School of Basic Medical Sciences, Key Laboratory of Molecular Cardiovascular Science of the Ministry of Education, Center for Non-coding RNA Medicine, Peking University Health Science Center, Beijing 100191, China
[b] Department of Hepatobiliary Surgery, Xi-Jing Hospital, Fourth Military Medical University, Xi'an 710032, China
[c] Department of Cardiology, Institute of Vascular Medicine, Peking University Third Hospital, Key Laboratory of Molecular Cardiovascular Science of the Ministry of Education, Beijing 100191, China
[d] Department of Central Laboratory and Institute of Clinical Molecular Biology, Peking University People's Hospital, Beijing 100044, China

ARTICLE INFO

Keywords:
FAM3A
ATPS
ATP production
Glucose and lipid metabolism

ABSTRACT

Reduced mitochondrial ATP synthase (ATPS) capacity plays crucial roles in the pathogenesis of metabolic disorders. However, there is currently no effective strategy for synchronously stimulating the expressions of ATPS key subunits to restore its assembly. This study determined the roles of mitochondrial protein FAM3A in regulating the activity and assembly of ATPS in hepatocytes. FAM3A is localized in mitochondrial matrix, where it interacts with F1-ATPS to initially activate ATP synthesis and release, and released ATP further activates P2 receptor-Akt-CREB pathway to induce FOXD3 expression. FOXD3 synchronously stimulates the transcriptions of ATPS key subunits and assembly genes to increase its assembly and capacity, augmenting ATP synthesis and inhibiting ROS production. FAM3A, FOXD3 and ATPS expressions were reduced in livers of diabetic mice and NAFLD patients. FOXD3 expression, ATPS capacity and ATP content were reduced in various tissues of FAM3A-deficient mice with dysregulated glucose and lipid metabolism. Hepatic FOXD3 activation increased ATPS assembly to ameliorate dysregulated glucose and lipid metabolism in obese mice. Hepatic FOXD3 inhibition or knockout reduced ATPS capacity to aggravate HFD-induced hyperglycemia and steatosis. In conclusion, FAM3A is an active ATPS component, and regulates its activity and assembly by activating FOXD3. Activating FAM3A-FOXD3 axis represents a viable strategy for restoring ATPS assembly to treat metabolic disorders.

1. Introduction

It has been estimated that >500 million people are suffering from type 2 diabetes worldwide at present [1]. Increased hepatic glucose production particularly gluconeogenesis is the central event in the development of hyperglycemia and type 2 diabetes [2,3]. Meanwhile, fatty liver disease is highly associated with increased hepatic gluconeogenesis and diabetes [4]. Mitochondrial dysfunction including the

Abbreviations: AMPK, adenosine 5′-monophosphate (AMP)-activated protein kinase; ATP, adenosine triphosphate; ATP11, ATPS mitochondrial F1 complex assembly factor 1; ATP12, ATPS mitochondrial F1 complex assembly factor 2; ATP23, mitochondrial inner membrane protease ATP23 homolog; ATP6, ATPS Fo subunit 6; ATPS, ATP Synthase; ATPSb, ATPS b subunit; ATPSc, ATPS c subunit; ATPSd, ATPS d subunit; ATPSα, ATPS α subunit; ATPSβ, ATPS β subunit; ATPSγ, ATPS γ subunit; ATPSδ, ATPS δ subunit; ATPSε, ATPS ε subunit; CaM, calmodulin; ChIP, chromatin immunoprecipitation; CHO, cholesterol; CoIP, Co-Immunoprecipitation; Complex IV, cytochrome *c* oxidase subunit IV; CREB, cAMP response element binding protein; DNP, 2,4-dinitrophenol; EPA, eicosapentaenoic acid; FAM3, family with sequence similarity 3; FCCP, carbonylcyanide-*p*-trifluoromethoxyphenylhydrazone; FFAs, free fatty acids; FOXD3, forkhead box protein D3; FOXO1, forkhead box protein O1; HCC, hepatocellular carcinoma; HFD, high fat diet; ITT, insulin tolerance tests; MMP, mitochondrial membrane potential; NAFLD, non-alcoholic fatty liver disease; ND, normal diet; OGTT, oral glucose tolerance tests; pAkt, phosphorylated Akt; PEPCK, phosphoenolpyruvate carboxykinase; PTT, pyruvate tolerance tests; ROS, reactive oxygen species; SDS, sodium dodecyl sulfonate; TG, triglyceride; TMEM70, transmembrane protein 70; TOM20, translocase of the outer membrane 20.

* Corresponding authors.
E-mail addresses: chiyujing@bjmu.edu.cn (Y. Chi), yangj@bjmu.edu.cn (J. Yang).
[1] These authors contributed equally to this work.

https://doi.org/10.1016/j.metabol.2022.155372
Received 25 August 2022; Accepted 25 November 2022
Available online 5 December 2022
0026-0495/

reduction of adenine triphosphate (ATP) synthesis and the increase of reactive oxygen species (ROS) production plays decisive roles in triggering insulin resistance, diabetes and steatosis [5–7]. A decrease in hepatic ATP content is highly correlated with insulin resistance, steatosis and hyperglycemia in obese and/or diabetic humans and animals [8–13]. Beyond metabolic disorders, mitochondrial dysfunction also plays crucial roles in the pathogenesis of many other diseases [14].

The majority of ATP is generated by mitochondrial ATP synthase (ATPS) [15], which is composed of Fo and F1 parts, and several other ancillary factors. Fo part (Fo-ATPS), which mainly consists of b, c and d subunits, is embedded in the inner membrane of mitochondria, while F1 part (F1-ATPS), which mainly consists of α, β, γ, δ and ε subunits, is located in the matrix of mitochondria and takes the responsibility for ATP synthesis [16,17]. ATPS synthesizes ATP using the proton gradient across the intermembrane space and matrix of mitochondria. A decrease in ATPS capacity impairs ATP synthesis ability and increases mitochondrial membrane potential (MMP, Δψ) to generate excessive ROS as evidenced by mutations in ATPS subunit genes in cultured human fibroblasts [18]. The β subunit (ATPSβ) is the catalytic subunit of ATPS [16,17]. ATPSβ expression and ATPS capacity were reduced in the livers of diabetic and steatotic animals [19–21]. Hepatic overexpression of ATPSβ elevated ATP production and release, and released ATP activated P2 receptor-Ca^{2+}-Calmodulin (CaM) pathway independent of insulin to suppress gluconeogenesis and lipogenesis, ameliorating hyperglycemia and steatosis of obese diabetic mice [21]. Although reduced ATP production is tightly associated with metabolic disorders, it is difficult to restore ATPS assembly for treating them due to the complexity of ATPS complex, which consists of up to 17 types of different subunits including F1/Fo part and ancillary factors [22]. So far, there is no confident strategy for simultaneously stimulating the expressions of ATPS key subunits and assembly factors to restore ATPS assembly and capacity under physiological conditions.

Family with sequence similarity 3 (FAM3) gene family consists of four members designated as FAM3A, FAM3B, FAM3C and FAM3D, respectively [23]. FAM3A is a new mitochondrial protein that enhances ATP production. Hepatic overexpression of FAM3A reversed hyperglycemia and steatosis of obese diabetic mice, whereas hepatic FAM3A inhibition caused hyperglycemia and lipid deposition in normal mice [24,25]. FAM3A activates ATP-P2 receptor-CaM-Akt pathway independent of insulin to suppress gluconeogenesis in hepatocytes [24,25]. FAM3A activation also ameliorates steatosis in obese mice [24,25]. Under obese condition, free fatty acids activate miR-423-5p to repress FAM3A expression, causing hepatic gluconeogenesis and steatosis [25]. Our previous studies have established that hepatocyte-released ATP is an important signaling molecule that suppresses gluconeogenesis and reduces lipid deposition [21,24–27]. Inhibition of miR-423-5p to increase FAM3A expression is involved in exercise-induced improvement of hyperglycemia in diabetic animals [28]. FAM3A also plays important roles in regulating the functions of adipocytes, pancreatic beta cells and vascular smooth muscle cells (VSMCs) by stimulating ATP production and release [29–33]. Moreover, FAM3A protects various cell types against oxidative-induced death by improving mitochondrial dysfunctions and reducing ROS production [25,34–37]. Anti-depressive drug doxepin [27] and imipramine [38] activates FAM3A pathways to ameliorate hyperglycemia and steatosis in obese animals. Clearly, FAM3A plays important roles in regulating many biological processes by modulating mitochondrial ATP synthesis. However, the mechanism(s) of FAM3A in stimulating mitochondrial ATP production remains unrevealed, which greatly restricts the understanding on its in-depth roles and mechanisms in various biological processes.

This study aimed to determine whether FAM3A regulated mitochondrial ATP synthesis by modulating the assembly and activity of ATPS.

2. Materials and methods

Animals - 8–10 weeks of male C57BL/6J mice, 8–12 weeks of male db/db and db/m mice with the BKS background were used in this study. C57BL/6J mice were fed on 45 % high fat diet (HFD) or normal diet (ND) for 12 weeks to induce diabetic and steatotic phenotype. $FAM3A^{-/-}$ mice were generated using TALEN technology in previous study [25], and male $FAM3A^{-/-}$ mice were used in the current study. All procedures involving experimental animals were approved by the Institutional Animal Care and Use Committee of Peking University Health Science Center (LA2018179).

Plasmid information - FOXD3 plasmid (c-Myc-Flag tag) was purchased from OriGene China (Cat No. MR222218), CREB1 plasmid (c-6 × His tag) was purchased from Mailgene Biosciences China (NM_004379.4), and FAM3A plasmid (c-6 × His-Flag tag) was purchased from WZ Biosciences Inc. China (NM_021806). The mutant plasmids of FAM3A (c-6 × His-Flag tag) were constructed by Shanghai Generay Biotech Co., Ltd (China). Adenovirus expressing FOXD3 was constructed by BAC Biological Technology Co., Ltd (China).

Adenoviral overexpression of FOXD3 in HFD mouse livers - 1.0×10^9 pfu Ad-FOXD3 or Ad-GFP were injected into tail vein of C57BL/6J mice after feeding on 45 % HFD or ND for 12 weeks. Oral glucose tolerance tests (OGTT), insulin tolerance tests (ITT) and pyruvate tolerance tests (PTT) were performed at 7 days and 14 days after injection, respectively. The mice were sacrificed at the fifteenth day. The serum and tissues were collected for biochemical analyses.

Construction of AAV-shFOXD3 - Three shRNA sequences targeting on CDS region of mice FOXD3 (shRNA1: GCACCACGTCGCTCATCAATTCAAGAGATTGATGAGCGACGTGGTGCTTTTTT, shRNA2: GCCTGCAGCTACAGCTCAACATTCAAGAGATGTTGAGCTGTAGCTGCAGGCTTTTTT, shRNA3: AGACGGCGCTGATGATGCATTCAAGAGATGCATCATCAGCGCCGTCTTTTTTT) were cloned into a pAV-3in1-shRNA-GFP vector under the U6 promoter and packaged into adeno-associated virus 8 (AAV-shFOXD3), the empty AAV-GFP virus served as control (WZ Biosciences Inc., China).

Adeno-associated viral inhibition of FOXD3 in ND or HFD mouse livers - 8-week C57BL/6J male mice were divided into 4 groups based on OGTT. 5×10^{11} vg AAV-shFOXD3 or AAV-GFP were injected into tail veins of mice. These mice fed on 45 % high fat diet (HFD) or normal diet (ND) for 14 weeks. OGTT, ITT and PTT were performed at different time points after injection to monitor the metabolic phenotype changes. Then mice were sacrificed, then the serum and tissues were collected for biochemical analyses.

Generation of mice with liver-specific deletion of FOXD3 gene - Two Loxp sites were inserted on both ends of exon 1 (the only exon) of mouse FOXD3 gene by Cyagen Biosciences Inc. (China). FOXD3-Loxp ($FOXD3^{fl/fl}$) mice on a C57BL/6J background were crossed with mice specifically expressing Cre in livers promoted by Albumin promoter (Alb-Cre) to generate mice with specific deletion of FOXD3 in hepatocytes ($FOXD3^{hep-/-}$).

Cell culture - HepG2 cells and 293T cells were cultured in DMEM medium (Gibco) supplemented with 10 % fetal bovine serum (Hyclone), 2 mM L-glutamine, 100 units/mL penicillin, and 100 units/mL streptomycin in incubator at 37 °C with 5 % CO_2. Cells were infected with 50 MOI Ad-GFP or Ad-FAM3A, Ad-ATPSβ and Ad-FOXD3 for 24 h with or without P2 receptors inhibitor suramin (50 μM). After 24 h, protein or RNA were collected for subsequent experiments. All cell lines were routinely tested for mycoplasma presence using a PCR detection kit (MP0035, Sigma).

Plasmid transfection - Cells were plated in 6-well plates the day before transfection, when the cells grow to about 50 % in the plates, replace with fresh medium, cells were transfected with 2 μg CREB plasmid, FAM3A plasmid or its mutations (His tag) for 24 h using

vigofect (T001, Vigorous Biotechnology, China), the same concentration of GFP plasmid was used as a negative control.

Western blotting assays - Protein samples were separated by SDS-PAGE and transferred to a nitrocellulose membrane. After overnight incubation with primary antibodies, membranes were washed and incubated with HRP-conjugated secondary antibodies (Biodragon, China) and then were detected using chemiluminescence kit (Santa Cruz Biotechnology, USA). Anti-FAM3A (SAB1102488, Sigma-Aldrich Inc., Germany), Anti-ATPSβ (ab14730), anti-FOXD3 (ab107248) and anti-Fatty Acid Synthase (ab22759) antibodies were from Abcam (U·K). Anti-EIF5 (A6583), anti-CREB1 (A1189) and anti-phospho-CREB1-S133 (AP0019) antibodies were from Abclonal (China). Anti-phospho-Akt-Ser473 (4060S), anti-Akt (9272S), anti-FOXO1 (2880S), and anti-phospho-FOXO1-S256 (9461S) antibodies were from Cell Signaling Technology, Inc. (MA). Anti-His-Tag and anti-C-Myc-Tag antibodies were from Biodragon (China). Anti-PEPCK (BS6870) antibody was from Bioworld (USA). Anti-G6Pase (sc-25840) antibody was from Santa Cruz Biotechnology, Inc. (USA). Anti-ATP11 (18016-1-AP) was from Proteintech (USA). Anti-Complex IV (bsm-33037M) was from Bioss (China).

Extraction of mitochondrial fractions - Extraction of mitochondria was performed according to the instructions for the Mitochondria/Cytosol Isolation Kit (C1260-100, Applygen Technologies, China). 100–200 mg of fresh mouse liver tissues or 2–5 × 10^7 cells homogenized in the ice-cold Mito Solution buffer, and centrifuged for 5 min at 4 °C, 800*g*. The supernatant was collected and centrifuged at 4 °C, 12,000*g* for 10 min. 1 mg mitochondria pellet was re-suspended with 40 μL T10E20 buffer (containing 10 mM Tris-HCl and 1 mM EDTA, pH 7.6) then added 10 μL (0.1 mg) digitonin. After mixing, 150 μL 250 mM sucrose solution was added in, mixed, and then centrifuged at 4 °C, 12,000*g* for 15 min. The pellet contained the mitochondrial inner membrane and matrix components, and the supernatant contained the mitochondrial outer membrane and intermembrane space components [39].

Analysis of ATPS complex - Mitochondrial protein was extracted using Mitochondria Isolation Kit mentioned above, and native-PAGE plus western blotting assay was performed to measure F1/Fo-ATPS complex [40]. Briefly, 50 μg mitochondrial proteins were separated by native-PAGE, and then transferred to a nitrocellulose membrane. After overnight incubation with anti-ATPSβ antibodies, membranes were washed and incubated with HRP-conjugated secondary antibodies (Biodragon, China), then detected using chemiluminescence kit (Santa Cruz Biotechnology, USA). Complex IV was probed as loading control. The estimated molecular weight of F1/Fo-ATPS complex is about 600 kD, and that of Complex IV is about 166 kD [40].

Reactive oxygen species detection - HepG2 cells and primary mouse hepatocytes infected with viruses for 24 h were washed with PBS twice after treatment and incubated with PBS containing 20 μM DCFH-DA [41] (Reactive oxygen species Assay Kit, Nanjing Jiancheng Bioengineering Institute, China) for 30 min. After washed twice with PBS, cells resuspended with PBS were sent to flow cytometry assay to detect the level of reactive oxygen species. The value was normalized to the control value.

Mitochondrial membrane potential detection - HepG2 cells and primary mouse hepatocytes infected with viruses for 24 h were washed with PBS twice after treatment and incubated with PBS containing 100 nM TMRM [42] (Invitrogen, USA) for 30 min. After washed twice with PBS, cells resuspended with PBS were sent to flow cytometry assay to detect the level of mitochondrial membrane potential. The value was normalized to the control value.

Measurement of mitochondrial ATP synthase activity - Mitochondrial Complex V activity was detected as previously described [43,44]. Briefly, mitochondria were isolated using the Mitochondria/Cytosol Fractionation Kit mentioned above from HepG2 cells. Mitochondrial precipitation was diluted in 250 mM sucrose and 2 mM EDTA (pH 9.0), and subjected to ultrasonic sonication. 100 or 200 ng/mL recombinant human FAM3A protein (TP303495, OriGene, USA) or solvent (25 mM Tris-HCl, 100 mM glycine, 10 % glycerol, pH 7.3) was added into the same amount of mitochondrial suspension, and incubated for 15 min at room temperature. ATP synthase activity was determined using the commercial kit (A089-5-1, Nanjing Jiancheng Bioengineering institution, China) to detect the NADH oxidation by spectrophotometer at 340 nm following the manufacturer's instructions.

Measurement of superoxide dismutase (SOD) activity - HepG2 cells or primary mouse hepatocytes infected with viruses for 24 h, or wide type and FAM3A-deficient hepatocytes were washed with PBS twice, and then lysed and detected by the SOD assay kit (BC0175, Solarbio, China) according to manufacturer's instruction [45]. The activity was normalized with the protein content in each sample (U/mg·protein).

Real-time PCR assays - Real-Time PCR was performed using Stastagene Mx3000P real-time quantitative PCR system (Agilent Technologies). Target gene mRNA level was normalized to β-actin of the same sample. All primer sequences were provided in Supplemental Table 1.

siRNA transfection - For CREB1 or FOXD3 knockdown, cells were treated with 50 nM siRNA mixture against human CREB1 or mouse FOXD3 mRNA (Beijing Biolino Nucleic Acid Technology Co., Ltd, China) for 24 h (The same concentration of scrambled siRNAs was used as negative control) before experimental assays. Or the cells were transfected with siRNAs for 6 h, followed by infection with viruses for 24 h. All the siRNA sequences were listed in Supplemental Table 2.

Luciferase reporter assay - The human ATPSβ and FOXD3 gene promoter fragments flanking −2000 bp to 0 bp were cloned into the pGL3-basic vector, respectively. The positive clone was selected and confirmed by DNA sequencing. The activation of firefly luciferase and ranilla luciferase were measured with the Dual-Luciferase reporter assay kit (Promega, USA) at 24 h after transfection as detailed previously [25].

Co-Immunoprecipitation (CoIP) - CoIP was performed using Pierce Crosslink Immunoprecipitation Kit (#26147, Thermo, USA) following the protocol in HepG2 cells as detailed in our previous reports [46].

GST Pull Down - Human FAM3A (NM_021806), ATP5A1 (NM_001001937), ATP5B (NM_001686) and ATP5G1 (NM_005175) genes were synthesized by WZ Biosciences Inc. (Shandong, China), and cloned to pGEX-4T-1 or pET-28a vector to make pET-28a-ATPSα/β/c-His or pGEX-4T-1-FAM3A-GST recombinant plasmid, respectively. Then the recombinant plasmids were expressed in *E. coli* BL21 (DE3) to obtain the fusion protein. The protein extract supernatant containing His-tag fusion protein (ATPSα/β/c-His) were purified by Ni-agarose resin, and replaced into desalting buffer (20 mM Tris, 150 mM NaCl, 5 mM EDTA, 1 mM DTT, 5 % GLY, pH = 8.0) by ultrafiltration centrifugation tube. The null-GST or FAM3A-GST fusion protein were immobilized on glutathione-sepharose resin, then incubated with purified ATPSα/β/c protein in desalting buffer at 4 °C rotating overnight separately. GST-elution buffer (20 mM Tris, 150 mM NaCl, 10 mM GSH, 1 mM DTT, pH = 8.0) was used to elute the resin, then performed with western blotting assays to detect the interaction.

Chromatin immunoprecipitation (ChIP) - HepG2 cells were washed with warm PBS twice and then fixed with 1 % formalin for 10 min at 37 °C. Wash and collect the cells using cold PBS, centrifuge at 3000 rpm for 10 min at 4 °C. Discard the flow-through. Dissolve the cells with 300 μL lysis buffer and incubate on ice for 10 min. Centrifuge the lysate at 14,000*g* for 10 min then collect the flow-through. Pre-clear lysate using the Control Agarose Resin and Salmon sperm DNA for 2 h. Centrifuge the lysate at 1000 rpm for 5 min then collect the flow-through. Add 2 μg antibody (anti-FOXD3/CREB, normal IgG as control) to the lysate and then incubate column with gentle end-over-end mixing or shaking overnight at 4 °C. Add agarose resin and salmon sperm DNA to the lysate and then incubate column at 4 °C for 2 h. Centrifuge at 1000 rpm for 5 min and discard the flow-through. Wash sample once with TSEI, TSEII, TSEIII and TE in turn. Add 100 μL of elution buffer and centrifuge. Put the final sample on 65 °C for 6 h to isolate the protein and DNA. Extract the DNA with phenol, chloroform and isoamyl alcohol. Agarose gel electrophoresis was performed after PCR. The primer sequences used in this research were provided in

Supplemental Table 3.

Mitochondrial respiration measurement - O_2 consumption rate in HepG2 cells was measured at 25 °C using the OROBOROS Oxygraph-2K (Innsbruck, Austria). In brief, wash the holes and add 2 mL DMEM to the holes. Pull up the plugs, and balance for about 30 min to ensure that the O_2 consumption rate was close to zero. Press the plug, balance for 10 min. HepG2 cells were collected after 24-h viral infection. Add the cells to pole A and B respectively, followed by treatment with 1 μM oligomycin (Selleck #S1478, inhibitor of mitochondrial ATPS), and 0.05–0.4 μM carbonylcyanide-*p*-trifluoromethoxyphenylhydrazone (FCCP, Selleck #S8276, a protonophoric uncoupler), and 0.5 μM antimycin A (Sigma #A8674) together with 0.5 μM rotenone (Selleck #S2348).

ATP content measurement - ATP was assayed using Bioluminescence assay using ATP Assay Kit according to manufacturer's instruction as detailed previously [25]. For determination of intracellular and extracellular ATP content, the absolute ATP values were measured and normalized with protein content, and then normalized to control values.

Glucose production Assay - HepG2 cells or primary mouse hepatocytes were infected with Ad-GFP or Ad-FOXD3 for 30 h in the absence or presence of suramin (50 μM) and then washed by PBS for three times. Glucose production protocol was detailed previously [25,47]. The glucose content was detected using Glucose Assay Kit (Sigma-Aldrich, GAGO-20) and normalized with protein content in each sample (μg/mg·protein).

Human liver samples - The physiological and biochemical characteristics of NAFLD patients and HCC patients were detailed previously [48]. The application for patient derived materials was approved by the Research Ethics Committee of Xijing Hospital, the Fourth Military Medical University (Ethics Number KY20172013-1) [48].

Cells neutral lipid staining - Cells plated on coverslips were infected with adenovirus in the presence of FFAs (0.2 mM oleic acid and 0.4 mM palmitic acid) and suramin (50 μM) for 24 h. Cells were washed with PBS for 3 times, and fixed with 4 % paraformaldehyde for 10 min. Cells were stained with LipidTOX™ neutral lipid stain (Invitrogen) for 30 min at room temperature away from light. After nuclear staining with DAPI for 1 h, coverslips were washed and mounted on glass slides. The cells on coverslips were visualized and imaged by fluorescence microscopy using Confocal Laser Scanning Microscope. TG content in the cells was determined using TG detection kit (E1013, Applygen, China) according to the manual.

Magnetic resonance imaging (MRI) - Mice were anesthetized using isoflurane and imaged in a horizontal position. The body of each animal was plain-scanned into 18-slice and the body composition was assessed by 3.0T MRTRIOTIM (SIEMENS) using NUMARIS/4, version syngo MR B17. The signals of liver fat or whole body fat were scratched and analyzed for lipid quantitation. The middle part of the body covering 8-

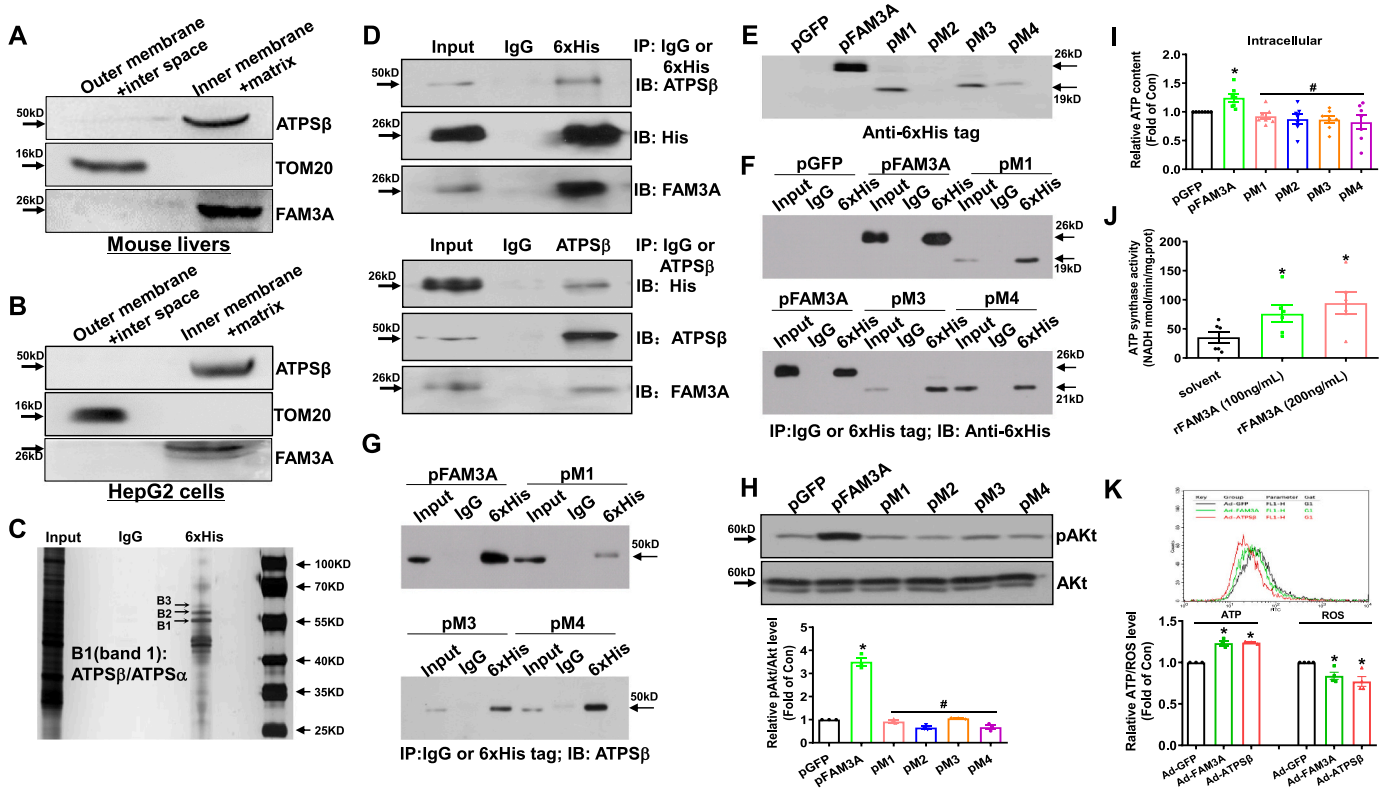

Fig. 1. FAM3A protein is localized in the matrix of mitochondria, and interacts with ATPS to regulate its activity. A–B) FAM3A is localized in the inner membrane/matrix of mouse livers (A) and HepG2 cells (B). The outer membrane/inter space and inner membrane/matrix were isolated as detailed in the experimental procedure. F1-ATPSβ and TOM20 were used as biomarkers for matrix and outer membrane fractions, respectively. C) Identification of proteins that potentially interacted with FAM3A in HepG2 cells. Hepatocytes were transfected with 6 × His tagged FAM3A plasmid for 24 h before CoIP was performed. Several protein bands were analyzed by mass spectrometry. B1–3, bands 1–3. ATPS alpha and beta subunits (ATPSα and ATPSβ) were among the potential proteins of Band 1. D) FAM3A interacted with ATPSβ as confirmed by CoIP and immunoblotting assays. HepG2 cells were transfected with 6 × His tagged FAM3A expression plasmid for 24 h before immunoprecipitation was performed. E) Characterization of mutant FAM3A expression in HepG2 cells. M1-M4, mutant FAM3A plasmids 1–4. F–G) Characterization of interactions between mutant FAM3A proteins and ATPSβ in HepG2 cells. The images shown above were the representatives of 3 independent experiments. H–I) Mutant FAM3A proteins failed to activate Akt (H) and induce ATP production (I) in HepG2 cells. Cells were transfected with wild type and mutant FAM3A plasmids for 24 h before experimental assays. N = 3–5, $^*P < 0.05$ versus pGFP-transfected cells. J) Recombinant FAM3A protein activated ATP synthase activity in isolated mitochondria from HepG2 cells. rFAM3A, recombinant human FAM3A protein. N = 6, $^*P < 0.05$ versus solvent. K) Overexpression of FAM3A and ATPSβ similarly increased intracellular ATP production and repressed ROS production in HepG2 cells. ROS level was determined at 24 h post viral infection. Representative ROS measurement curve was shown in upper panel, and quantitative data was shown in lower panel. N = 3–4, $^*P < 0.05$ versus Ad-GFP-infected cells.

slice images was chosen as representative images in the figure.

Statistical analysis - The results are analyzed using Graphpad Prism 8.0 (GraphPad Prism Software, Inc., San Diego, CA) and presented as mean ± SEM. Statistical significance of differences between groups was analyzed by *t*-test or ANOVA for the normal distributed data. Non-normal distributed data were calculated by Mann-Whitney *U* test (two groups) or Kruskal-Wallis test (multiple groups). *P* values < 0.05 were considered as statistically significant.

3. Results

FAM3A interacts with and activates F1-ATPS - We had previously demonstrated that FAM3A protein is mainly located in mitochondria of hepatocytes, pancreatic β cells, adipocytes and VSMCs [24,29–32]. Here we further showed that FAM3A protein is predominantly located in the inner membrane/matrix fraction of mitochondria in mouse livers and human hepatocytes (Fig. 1A–B). To determine whether FAM3A interacted with some protein(s), mouse FAM3A gene containing a 6 × His tag was overexpressed in HepG2 cells, and then CoIP was performed using anti-His antibodies. Several protein bands immunoprecipitated by anti-His antibodies were analyzed by mass spectrometry. Notably, mitochondrial ATPSβ and ATPSα, which located in the matrix of mitochondria and form F1-ATPS, were among the potential proteins identified for band 1 (Fig. 1C and Supplemental Table 4). Cross CoIP experiments confirmed that FAM3A indeed interacted with F1-ATPSβ (Fig. 1D). Moreover, anti-His antibodies also immunoprecipitated F1-ATPSα and Fo-ATPSc, the latter formed the pedestal of ATPS (Suppl Fig. 1A–B). CoIP using anti-FAM3A antibodies also immunoprecipitated F1-ATPSβ, F1-ATPSα and Fo-ATPSc in HepG2 cells and primary mouse hepatocytes (Suppl Fig. 1C–D). Moreover, FAM3A-ATPS interaction was increased after FAM3A overexpression in both human and mouse hepatocytes (Suppl Fig. 1C–D). Beyond hepatocytes, anti-FAM3A antibodies also immunoprecipitated F1-ATPSβ, F1-ATPSα and Fo-ATPSc in VSMCs and pancreatic β cells (Suppl Fig. 1E–F). Clearly, FAM3A interacts with the full ATPS in various cell types. Then, GST pulldown was performed to identify with which subunit of ATPS FAM3A directly interacted. As a result, FAM3A interacted with ATPSβ and ATPSα, but not ATPSc (Suppl Fig. 1G), indicating that FAM3A directly interacted with F1-ATPS. Given that ATPSβ was the catalytic subunit of ATPS, FAM3A-ATPSβ interaction was used to represent FAM3A-ATPS interaction in the following experiments. To determine whether FAM3A activated ATPS activity, a series of mutant FAM3As with different truncations had been constructed (Suppl Fig. 2). M1, M3 and M4 mutant FAM3A proteins could be effectively expressed in HepG2 cells (Fig. 1E). Although mutant FAM3A proteins were still capable of interacting with ATPSβ (Fig. 1F–G), they failed to increase intracellular ATP content and induce Akt phosphorylation in HepG2 cells (Fig. 1H–I). Notably, treatment with recombinant FAM3A protein activated ATPS activity in isolated mitochondria (Fig. 1J). FAM3A overexpression similarly increased intracellular ATP content, and reduced ROS production and MMP as ATPSβ overexpression in HepG2 cells (Fig. 1K and Suppl Fig. 3A) and primary mouse hepatocytes (Suppl Fig. 3B–D). In FAM3A-deficient hepatocytes, ATP production was decreased while MMP and ROS production were increased (Suppl Fig. 3E–G). Although FAM3A deficiency had little effect on the activity of antioxidant enzyme superoxide dismutase (SOD), FAM3A overexpression increased its activity in HepG2 cells and mouse hepatocytes (Suppl Fig. 3H–J). Collectively, FAM3A is a novel active component of ATPS, and activates ATPS activity by interacting with F1 part to enhance ATP production and reduce MMP, accompanied with an increase in SOD activity and decrease in ROS production.

FAM3A activated CREB-FOXD3 axis to regulate the transcription of ATPSβ - We had previously reported that the mRNA and protein levels of FAM3A [24] and ATPSβ [21] were reduced in the livers of obese diabetic mice, respectively (Suppl Fig. 4A–B). The consistent changes in FAM3A and ATPSβ mRNAs suggested that FAM3A may also regulate the transcription of ATPSβ gene beyond modulating its protein activity. To address this issue, the potential transcription factor binding sites in the promoters of human, mouse and rat ATPSβ genes were predicted using bioinformatic method. The prediction revealed that all of human, mouse and rat ATPSβ gene promoters had potential binding sites highly specific for the transcription factor Forkhead Box D3 (FOXD3) (Suppl Fig. 5). In contrast, there were no other common transcription factor binding sites in ATPSβ gene promoters across species (Suppl Fig. 5). Reference mining indicated that FOXD3 was a key transcription factor involved in organ development, and global knockout of FOXD3 gene caused embryo death in mice [49]. Mice with pancreatic β-specific knockout of FOXD3 gene exhibited impaired proliferation of β cells and glucose intolerance during pregnancy [50]. So far, the role of FOXD3 in hepatic glucose and lipid metabolism remained unknown. In mouse livers, FAM3A silencing reduced the mRNA and protein levels of FOXD3 (Fig. 2A–B). In contrast, FAM3A silencing had little effect on the mRNA levels of other predicted transcription factors including c-Rel and Pax-6 in mouse livers (Fig. 2A and Suppl Fig. 5). Moreover, the mRNA level of FOXD3 but not those of c-Rel and Pax-6 was reduced in HFD mouse livers (Fig. 2C). FOXD3 protein was reduced in the livers of obese mice (Fig. 2D). In FAM3A-deficient mouse livers and skeletal muscles, the expressions of FOXD3 and ATPSβ were reduced with decreased ATP content (Fig. 2E–J). The expressions of FAM3A, FOXD3 and ATPSβ were also reduced in liver samples of NAFLD patients when compared with those of HCC patients (Fig. 2K). As described previously, NAFLD patients had higher serum blood glucose and TG levels than HCC patients [48]. FAM3A-deficient mice exhibited glucose intolerance and insulin resistance (Suppl Fig. 6A–C). TG but not CHO content was increased in FAM3A-deficient mouse livers (Suppl Fig. 6D–F). Moreover, phosphorylated Akt (pAkt) level was decreased while gluconeogenic gene expressions were increased in FAM3A-deficient mouse livers (Suppl Fig. 6G). ATPS capacity was reduced in FAM3A-deficient mouse livers (Suppl Fig. 6H). We had recently demonstrated that anti-depressant imipramine activated FAM3A to ameliorate hyperglycemia and steatosis with increased hepatic ATP content in obese mice [38]. Here we showed that imipramine treatment increased ATPS capacity in obese mouse livers but not in FAM3A-deficient mouse livers (Suppl Fig. 6I).

To further determine whether FAM3A regulated ATPSβ expression via FOXD3, the impact of FAM3A overexpression on FOXD3 and ATPSβ expressions was firstly evaluated in cultured hepatocytes. In both HepG2 cells (Fig. 3A–B) and primary mouse hepatocytes (Fig. 3C–D), FAM3A overexpression upregulated the mRNA and protein levels of FOXD3 and ATPSβ. Then, whether FOXD3 directly regulated the expression of ATPSβ was evaluated. ChIP assays revealed that FOXD3 bound to the two potential binding sites in human ATPSβ gene promoter (Fig. 3E–F and Suppl Fig. 5). A 2 kb fragment of human ATPSβ gene promoter containing these two potential FOXD3 binding sites was cloned (Fig. 3F). FOXD3 activated the promoter activity of human ATPSβ gene in both 293T and HepG2 cells, and mutations of two potential FOXD3 binding sites abolished the activation effects of FOXD3 (Fig. 3G–H). Furthermore, bioinformatic analysis revealed that the promoters of mouse ATPSα subunit (ATPSα), ATPS γ subunit (ATPSγ) and ATPS c subunit (ATPSc) genes also contained several potential binding sites for FOXD3 (Suppl Fig. 7). FAM3A and FOXD3 overexpression upregulated the mRNA levels of ATPSβ and other key subunits of ATPS complex including ATPSα, ATPSγ, ATPSδ, ATPSε, ATPSc and ATPSd in mouse hepatocytes (Fig. 3I–J). Beyond F1Fo-ATPS genes, the mRNA levels of several ancillary factors which assisted the assembly of F1Fo-ATPS complex including ATPS subunit 6 (ATP6), ATPS mitochondrial F1 complex assembly factor 1 (ATP11), ATPS mitochondrial F1 complex assembly factor 2 (ATP12), mitochondrial inner membrane protease ATP23 homolog (ATP23) and transmembrane protein 70 (TMEM70) were also upregulate by FAM3A and FOXD3 overexpression in mouse hepatocytes (Suppl Fig. 8A–B). As expected, FAM3A and FOXD3 overexpression increased ATPS capacity in mouse and human hepatocytes (Fig. 3K–L).

Because it was difficult to determine whether FOXD3 directly

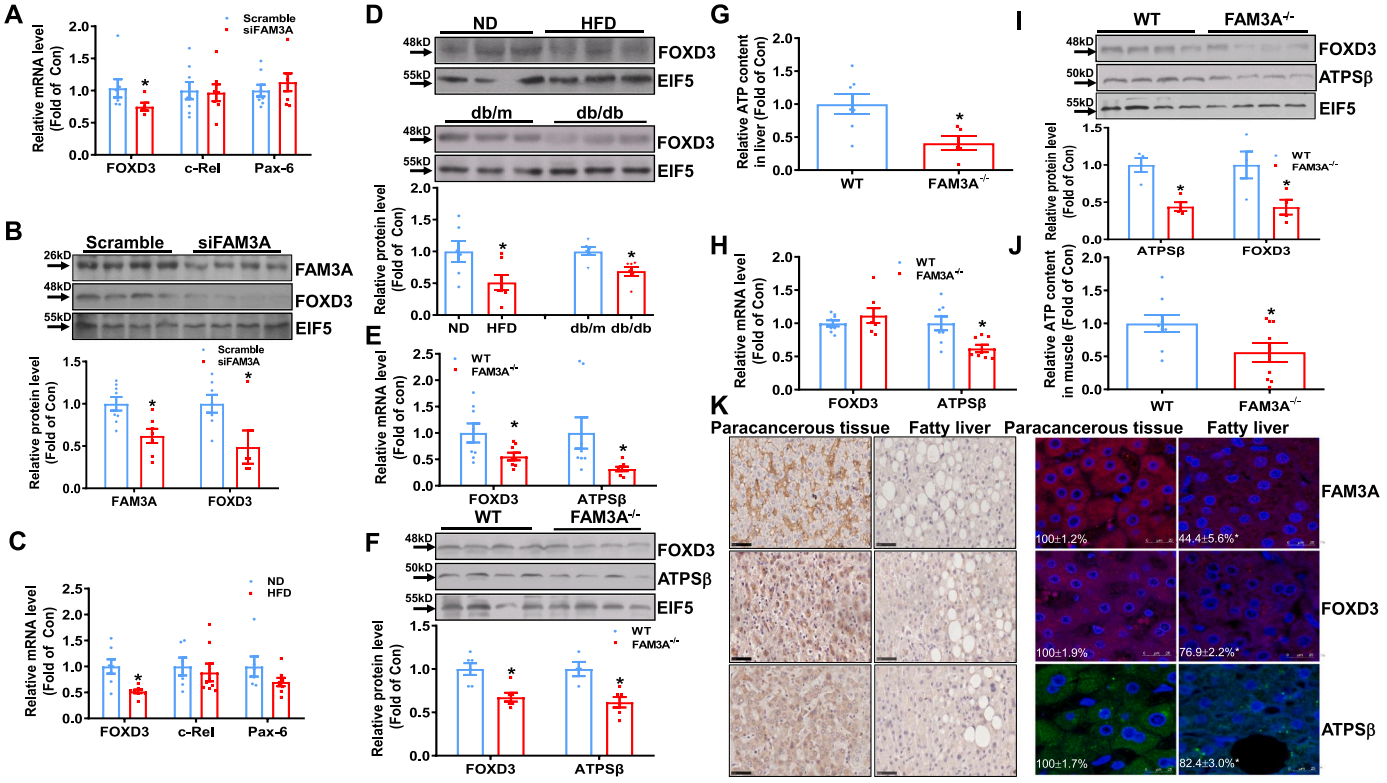

Fig. 2. Consistent changes of FAM3A and FOXD3 expressions in mouse livers. A–B) siRNA-mediated inhibition of FAM3A expression reduced the mRNA (A) and protein (B) levels of FOXD3 in normal mouse livers. N = 6–8, $^*P < 0.05$ versus scramble-treated mouse livers. C–D) FOXD3 mRNA (C) and protein (D) levels were reduced in the livers of obese mice. ND, normal diet; HFD, high fat diet. db/m, db/m mice, db/db, db/db mice. N = 5–6, $^*P < 0.05$ versus db/m or ND mouse livers. E–F) The mRNA (E) and protein (F) levels of FOXD3 and ATPSβ were reduced in FAM3A-deficient mouse livers. G) ATP content was reduced in FAM3A-deficient mouse livers when compared with wild type mouse livers. H–I) The mRNA (H) and protein (I) levels of FOXD3 and ATPSβ were reduced in skeletal muscles of FAM3A-deficient mice. 20-week old FAM3A$^{-/-}$ and wild type mice were used for experimental analysis. J) ATP content was reduced in FAM3A-deficient mouse skeletal muscle when compared with wild type mice. In panel E–J, FAM3A-deficient mice were sacrificed at 21 weeks old for experimental assays. N = 6–8, $^*P < 0.05$ versus wild type mice. K) The protein levels of FAM3A, FOXD3 and ATPSβ expressions were reduced in paracancerous liver tissues when compared with that of NAFLD patients as assayed by immunohistochemical staining (left panel) and immunofluorescent (right panel). Images were the representative staining of 3 sets of liver tissues. The relative fluorescence density was indicated in the representative images. N = 3, $^*P < 0.05$ versus paracancerous liver tissues.

regulated the transcriptions of all F1Fo-ATPS genes and ancillary factor genes of ATPS at the same time, and given that ATPSβ was the catalytic subunit of ATPS, whether FAM3A activated FOXD3 to induce ATPSβ expression in hepatocytes was further probed. Moreover, because ATP11 assisted the assembly of ATPSβ into F1-ATPS [22], whether FOXD3 regulated its expression was also evaluated. FOXD3 overexpression increased ATPSβ and ATP11 protein levels, and ATP content in mouse hepatocytes (Fig. 4A–B and Suppl Fig. 8C). In support, FOXD3 silencing reduced the mRNA levels of F1Fo-ATPS genes (Fig. 4C) and ancillary factor genes in mouse hepatocytes (Suppl Fig. 8D). FOXD3 silencing reduced ATPSβ and ATP11 protein levels, and ATP content in mouse hepatocytes (Fig. 4D–E and Suppl Fig. 8E). Bioinformatic analysis predicted one potential FOXD3 binding site (−1651 bp/−1647 bp) in mouse ATP11 gene, which was bound by FOXD3 as evidenced by ChIP assay (Suppl Fig. 8F).

Clearly, ATPSβ and ATP11 are the direct target genes of FOXD3. FOXD3 overexpression induced Akt and FOXO1 phosphorylation, and repressed gluconeogenic gene expression, but was inhibited by P2 receptor (ATP receptor) inhibitor suramin in mouse hepatocytes (Fig. 4F). Moreover, FOXD3 overexpression promoted the nuclear exclusion of FOXO1 and suppressed gluconeogenesis but was antagonized by suramin in mouse hepatocytes (Fig. 4G–H). In support, FOXD3 overexpression similarly increased ATPSβ protein level, ATP content and Akt phosphorylation, and suppressed gluconeogenesis in HepG2 cells (Suppl Fig. 9A–D). Mitochondrial function measurement further revealed that FOXD3 overexpression increased ATP synthesis rate in HepG2 cells (Fig. 4I–J). Moreover, FAM3A and FOXD3 overexpressions reduced MMP in HepG2 cells (Fig. 4K). With increased ATP production and decreased MMP, FOXD3 overexpression reduced ROS production in HepG2 cells (Fig. 4L), which was similar to the effects of FAM3A and ATPSβ overexpressions (Fig. 1K). Overexpressions of FAM3A, FOXD3 and ATPSβ comparably reduced free fatty acid-induced lipid deposition in P2 receptor-dependent manner in HepG2 cells (Fig. 4M–N). Moreover, AAV-mediated inhibition of FOXD3 blunted FAM3A-promoted increase in F1Fo-ATPS and assembly gene expressions, ATPS capacity and ATP production (Suppl Fig. 10A–E). FOXD3 inhibition also impaired FAM3A-induced suppression of lipid deposition and gluconeogenesis in mouse hepatocytes (Suppl Fig. 10F–H).

Because FAM3A and FOXD3 mRNAs were concomitantly changed in cultured hepatocytes and mouse livers, whether FAM3A regulated the transcription of FOXD3 was further probed. Bioinformatic prediction revealed that both human and mouse FOXD3 gene promoters contain potential binding sites for certain transcription factors including cAMP response element binding protein (CREB) (Suppl Fig. 11). Reference mining revealed that CREB can be phosphorylated and activated by Akt at Ser133 in various cell types [51,52]. In HepG2 cells, FAM3A-induced Akt activation was concomitant with CREB phosphorylation, but was inhibited by suramin (Fig. 5A). ChIP and luciferase reporter analyses revealed that CREB bound to and activated the promoter activity of human FOXD3 gene (Fig. 5B–C). Plasmid overexpression of CREB increased the mRNA and protein levels of FOXD3 and ATPSβ, and increased cellular ATP content in HepG2 cells (Fig. 5D–F). siRNA

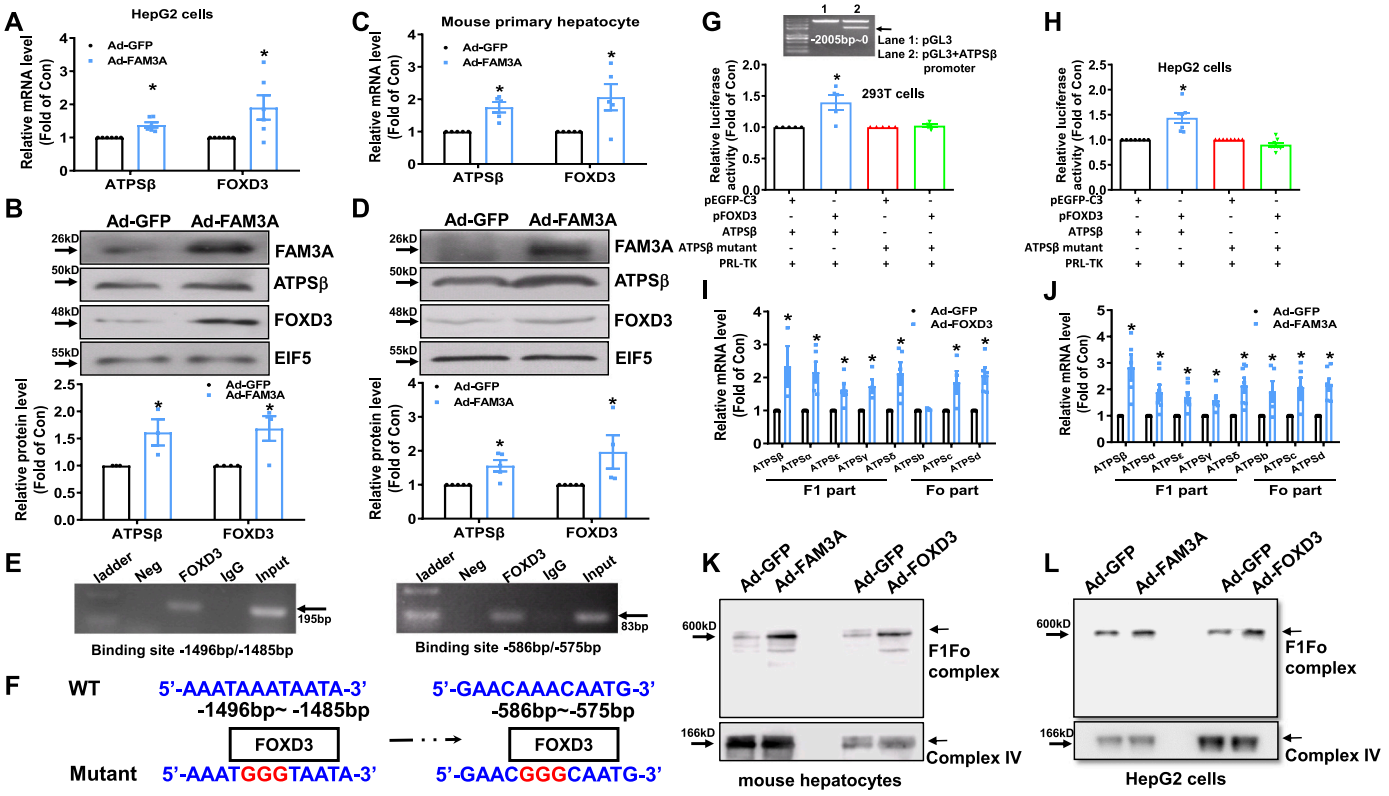

Fig. 3. FAM3A overexpression activated FOXD3 and ATPSβ expressions in cultured hepatocytes. A–B) FAM3A overexpression upregulated the mRNA (A) and protein (B) levels of FOXD3 and ATPSβ in HepG2 cells. N = 4–6, $^*P < 0.05$ versus Ad-GFP-infected control cells. C–D) FAM3A overexpression upregulated the mRNA (C) and protein (D) levels of FOXD3 and ATPSβ in primary mouse hepatocytes. N = 4–5, $^*P < 0.05$ versus Ad-GFP-infected control hepatocytes. E) ChIP assays revealed that FOXD3 bound to the potential sites in the promoter region of human ATPSβ gene. F) Generation of reporters driven by wild type and mutant human ATPSβ gene promoter. G–H) FOXD3 activated wild type but not mutant ATPSβ promoter reporter in both 293T (G) and HepG2 (H) cells. N = 5, $^*P < 0.05$ versus pGFP-transfected control cells. I–J) FOXD3 and FAM3A overexpressions on the mRNA levels of ATPS subunits in mouse hepatocytes. N = 5–7, $^*P < 0.05$ versus Ad-GFP-infected control cells. K–L) FAM3A and FOXD3 overexpressions increased ATPS capacity in mouse hepatocytes (K) and HepG2 cells (L). The gel images represented 3 independent experiments. The same amount of isolated mitochondria protein was subjected to Native-PAGE and western blotting assay using anti-ATPSβ antibodies as detailed in an experimental procedure. After ATPS complex assays, the membrane was stripped and Complex IV was assayed as loading control. Complex IV, cytochrome *c* oxidase subunit IV.

silencing of CREB inhibited FAM3A-induced increase in FOXD3 and ATPSβ expressions, and ATP production in HepG2 cells (Fig. 5G–H). Although silencing of CREB inhibited FAM3A-induced FOXD3 and ATPSβ upregulation, it failed to completely blunt FAM3A-induced ATP production in HepG2 cells (Fig. 5H), which was likely due to that FAM3A activated ATPS activity. In mouse hepatocytes, FAM3A-induced Akt and CREB phosphorylation, and FOXD3 and ATPSβ upregulation was reversed by suramin (Fig. 5I). Moreover, overexpression of mutant FAM3A proteins failed to upregulate FOXD3 and ATPSβ expressions in HepG2 cells (Fig. 5J). Collectively, FAM3A activated ATP-Akt-CREB pathway to stimulate FOXD3 expression, which induced the transcriptions of F1Fo-ATPS genes and assembly genes to increase ATPS capacity.

Modulation of hepatic FOXD3 expression on glucose and lipid metabolism - To further confirm the effects of FOXD3 on ATPS assembly, ATP production, and glucose and lipid metabolism in vivo, FOXD3 gene was overexpressed or inhibited in mouse livers. To overexpress FOXD3 in obese mouse livers, Ad-FOXD3 were injected via the tail veins. At 7 and 14 days post viral injection, glucose intolerance of HFD mice treated with Ad-FOXD3 was improved when compared with HFD mice treated with Ad-GFP (Fig. 6A–C). Injection of Ad-FOXD3 improved global insulin resistance and suppressed hepatic glucose production in HFD mice (Fig. 6D–E). Ad-FOXD3 injection attenuated fasting hyperglycemia of HFD mice At 7 and 14 days (Fig. 6F). Ad-FOXD3 injection also reduced lipid deposition and TG content in mouse livers (Fig. 6G–H). In contrast, it had little effect on hepatic CHO content (Fig. 6H). Moreover, Ad-FOXD3 injection reduced serum TG but not CHO levels (Fig. 6H). Injection of Ad-FOXD3 resulted in significant overexpression of FOXD3 mRNA in liver but not in other main metabolic tissues (Fig. 6I). FOXD3 overexpression increased ATP content and ATPS capacity in mouse livers (Fig. 6J–K). In mouse livers, FOXD3 overexpression upregulated the mRNA levels of F1Fo-ATPS subunits and ancillary factors, and decreased those of gluconeogenic and lipogenic genes (Fig. 6L and Suppl Fig. 12A). Ad-FOXD3 injection increased FOXD3 protein by about 3 folds in mouse livers (Fig. 6M). FOXD3 overexpression increased the protein levels of ATPSβ and ATP11, and phosphorylated Akt and FOXO1, while decreased those of gluconeogenic and lipogenic genes in mouse livers (Fig. 6M and Suppl Fig. 12B).

In the previous study, we had revealed that ATPSβ overexpression activated ATP-Akt pathway in mouse livers and cultured hepatocytes [21]. The previous and current findings suggested that FAM3A may initiate and control a novel regulation loop among ATP, Akt, CREB, FOXD3 and ATPS in hepatocytes. In support, although CREB directly regulated FOXD3 expression, FOXD3 overexpression also increased CREB phosphorylation in mouse livers concomitant with Akt activation (Fig. 6M–N). To further validate the ATP-Akt-CREB-FOXD3-ATPSβ regulation loop, the effects of ATPSβ overexpression on CREB phosphorylation and FOXD3 expression were further evaluated in cultured hepatocytes. As a result, ATPSβ overexpression induced Akt and CREB phosphorylation, and upregulated FOXD3 expression in mouse hepatocytes (Fig. 6O). ATPSβ overexpression also increased the mRNA levels of other F1Fo-ATPS subunits (Fig. 6P) and ancillary factors (data not shown) in mouse hepatocytes, which were consistent with the effects of

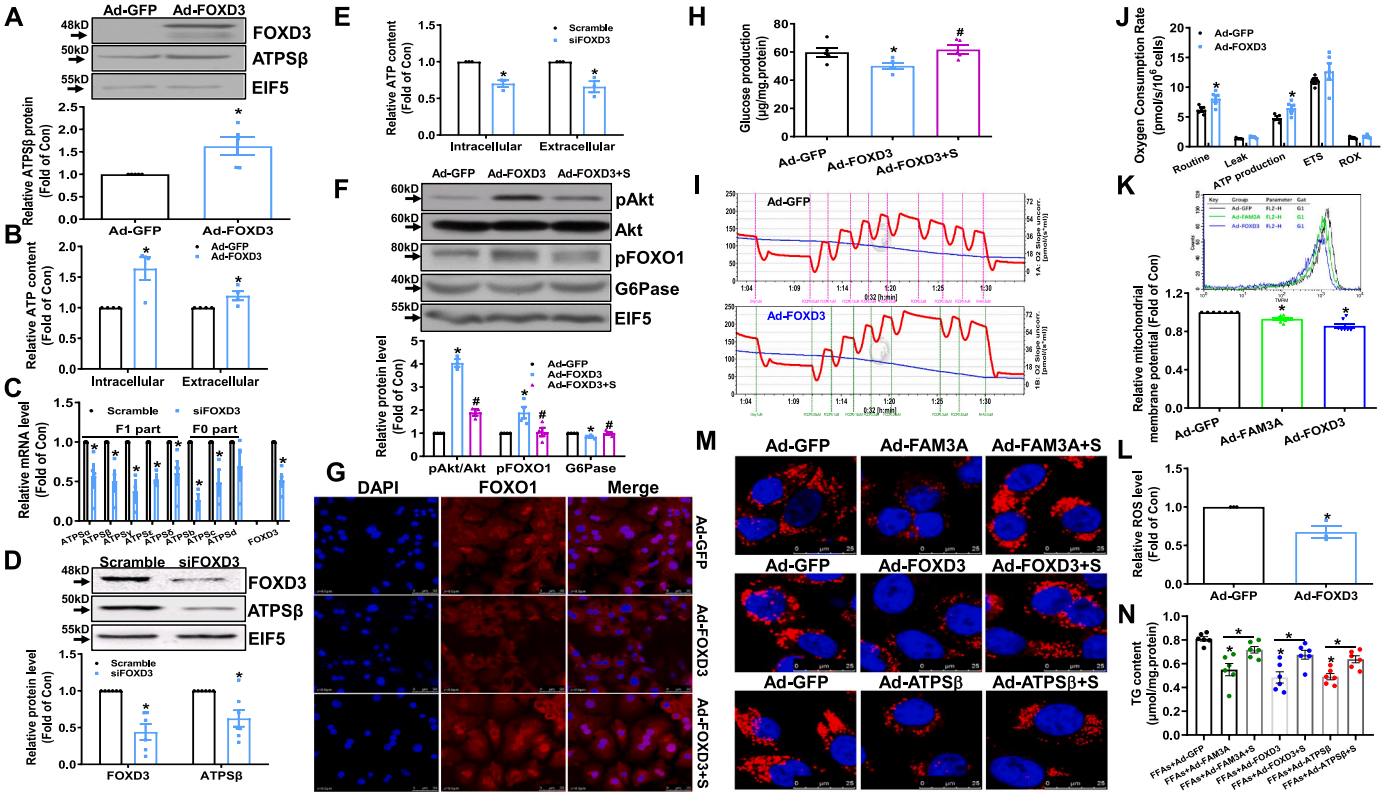

Fig. 4. FOXD3 upregulated ATPSβ to suppress gluconeogenesis in primary mouse hepatocytes. A–B) FOXD3 overexpression upregulated ATPSβ protein level (A) and increased ATP content (B) in mouse hepatocytes. N = 5, $^{*}P < 0.05$ versus Ad-GFP-infected control cells. C–E) FOXD3 silencing reduced the mRNA levels (C) of F1/Fo genes of ATPS, ATPSβ protein level (D) and ATP content (E) in mouse hepatocytes. N = 3–5, $^{*}P < 0.05$ versus control cells. F) FOXD3 activated Akt, phosphorylated FOXO1 and inhibited gluconeogenic gene expression in P2 receptor-dependent manner. G) FOXD3 promoted the nuclear exclusion of FOXO1 in P2 receptor-dependent manner. H) FOXD3 suppressed glucose production in P2 receptor-dependent manner. Ad-FOXD3 + S, hepatocytes were infected with Ad-FOXD3 in the presence of suramin for 24 h. N = 5, $^{*}P < 0.05$ versus Ad-GFP-infected control cells, $^{\#}P < 0.05$ versus Ad-FOXD3-treated cells. I–J) FOXD3 overexpression increased ATP synthesis rate in HepG2 cells. Representative mitochondrial function measurement curve was shown in panel I, and quantitative data shown in panel J. Routine: basal respiration; leak: proton leak; ETS: maximal respiration; ROX: non-mitochondrial respiration. ATP production was calculated by subtracting proton leak from basal respiration. N = 5, $^{*}P < 0.05$ versus Ad-GFP-infected control cells. K) Overexpression of FAM3A and FOXD3 reduced mitochondrial membrane potential in HepG2 cells. Representative potential measurement curve was shown in upper panel, and quantitative data shown in lower panel. L) Overexpression of FOXD3 reduced ROS production in HepG2 cells. M–N) Overexpression of FAM3A, FOXD3 and ATPSβ reduced FFAs-induced lipid deposition in P2 receptor-dependent manner in HepG2 cells. Representative confocal images were shown in panel M, and quantitative data in panel N. N = 6, $^{*}P < 0.05$ versus Ad-GFP-infected control cells, or between two indicated groups of cells.

FAM3A and FOXD3 overexpressions (Fig. 3I–J). Similarly, ATPSβ overexpression also induced CREB phosphorylation, and upregulated FOXD3 expression in HepG2 cells (Suppl Fig. 12C–D). Overall, these findings revealed a novel regulation loop among ATP, Akt, CREB, FOXD3 and ATPS in hepatocytes.

For inhibiting hepatic FOXD3 expression, AAV-shFOXD3 or AAV-GFP were injected via tail veins, and then the mice were fed on ND or HFD. After fed on HFD for 10 weeks, AAV-shFOXD3 group of mice exhibited more severe glucose intolerance when compared to AAV-GFP control mice (Fig. 7A). There was no significant difference between the two ND groups of mice. Moreover, fasting blood glucose, hepatic gluconeogenesis and insulin resistance were also aggravated in AAV-shFOXD3 group of mice when compared to AAV-GFP of mice (Fig. 7B–C). MRI analysis illustrated that hepatic FOXD3 inhibition increased liver fat deposition and global fat volume in HFD mice (Fig. 7D). Morphological analyses confirmed that FOXD3 inhibition increased liver weight and epididymal fat weight after HFD feeding (Fig. 7E). Because the distinct metabolic changes mainly occurred after HFD feeding, the following experiments focused on HFD-AAV-GFP and HFD-AAV-shFOXD3 groups of mice. H.E and Oil Red O staining revealed more severe hepatic lipid accumulation in AAV-shFOXD3 mice than in control mice (Fig. 7F–G). Quantitative analyses revealed that TG and CHO levels in liver but not in serum were increased in AAV-shFOXD3 mice (Fig. 7H). AAV-shFOXD3 injection reduced ATP content, ATPS capacity and the mRNA levels of FOXD3, ATPS key subunits and assembly factors in mouse livers (Fig. 7I–L). AAV-shFOXD3 injection reduced FOXD3 protein level, and suppressed the phosphorylation levels of Akt, FOXO1 and CREB, and ATPSβ protein level, while increased gluconeogenic and lipogenic protein levels (Fig. 7M).

To further confirm the long-term effects of FOXD3 in regulating ATPS assembly and glucose/lipid metabolism, FOXD3 was specifically deleted from hepatocyte. FOXD3-Loxp mice were generated and crossed with Alb-Cre mice to generate hepatic-specific FOXD3-knockout mice ($FOXD3^{hep-/-}$) (Suppl Fig. 13A). The genomic DNA and protein identifications of $FOXD3^{fl/fl}$ and $FOXD3^{hep-/-}$ mice were shown on Suppl Fig. 13B. $FOXD3^{fl/fl}$ and $FOXD3^{hep-/-}$ mice exhibited similar glucose intolerance under normal chow (data not shown), so they were subjected to HFD at the age of 8-week old. When compared to $FOXD3^{fl/fl}$ mice, $FOXD3^{hep-/-}$ mice exhibited increased hepatic gluconeogenesis, decreased insulin sensitivity, aggravated glucose intolerance and fasting hyperglycemia after fed on HFD for 10–14 weeks (Fig. 8A–D). MRI analysis illustrated that hepatic deletion of FOXD3 increased liver fat deposition and global fat volume (Fig. 8E). Morphological and quantitative analyses showed that $FOXD3^{hep-/-}$ mice had more abdominal fat accumulation and liver steatosis than $FOXD3^{fl/fl}$ mice (Fig. 8F–G). Oil Red O staining confirmed more severe hepatic lipid accumulation in

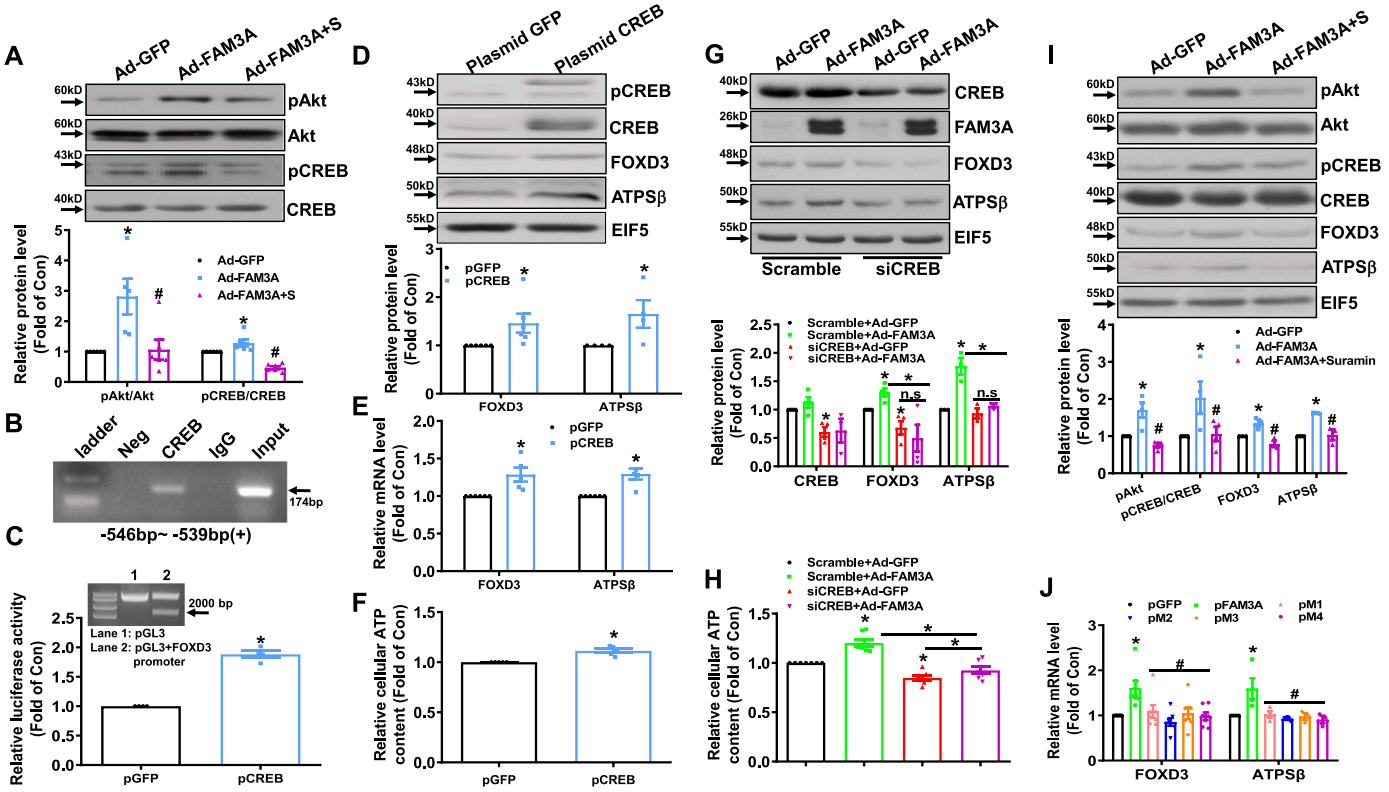

Fig. 5. FAM3A activated CREB to upregulate FOXD3 and ATPSβ expression in hepatocytes. A) FAM3A induced CREB activation in P2 receptor-dependent manner in HepG2 cells. Ad-FAM3A + S, hepatocytes were infected with Ad-FAM3A in the presence of suramin. N = 6, $^{*}P < 0.05$ versus Ad-GFP-infected control cells, $^{\#}P < 0.05$ versus Ad-FAM3A-treated cells. B) CREB bound with the promoter region of human FOXD3 gene as revealed by ChIP. C) CREB activated human FOXD3 promoter luciferase in HepG2 cells. Human FOXD3 promoter fragment flanking −2000 to 0 bp was cloned in to pGL3-basic vector as indicated in the gel image. D–E) Plasmid overexpression of CREB upregulated the protein (D) and mRNA (E) levels of FOXD3 and ATPSβ in HepG2 cells. F) CREB overexpression increased cellular ATP content in HepG2 cells. N = 4–6, $^{*}P < 0.05$ versus pGFP-transfected control cells. G) Silencing of CREB blunted FAM3A-induced expressions of FOXD3 and ATPSβ in HepG2 cells. Representative gel images were shown in upper panel, and quantitative data in lower panel. H) Silencing of CREB blunted FAM3A-induced ATP production in HepG2 cells. N = 3–5, $^{*}P < 0.05$ versus scramble + Ad-GFP group of cells, or between two indicated groups of cells. N.S, no significant difference between two indicated groups of cells. I) Inhibition of P2 receptor blunted FAM3A-induced upregulation of FOXD3 and ATPSβ in mouse hepatocytes. Representative gel images were shown in upper panel, and quantitative data in lower panel. N = 4, $^{*}P < 0.05$ versus Ad-GFP-infected control cells, $^{\#}P < 0.05$ versus Ad-FAM3A-treated cells. J) Mutant FAM3A proteins failed to affect the mRNA levels of FOXD3 and ATPSβ in HepG2 cells. N = 4–7, $^{*}P < 0.05$ versus pGFP-transfected control cells, $^{\#}P < 0.05$ versus pFAM3A-transtreated cells.

FOXD3$^{hep-/-}$ mice than in FOXD3$^{fl/fl}$ mice (Fig. 8H). Quantitative analysis revealed that both liver and serum TG levels were significantly elevated in FOXD3$^{hep-/-}$ mice, while CHO levels in serum but not in livers were increased in FOXD3$^{hep-/-}$ mice (Fig. 8I). Moreover, hepatic FOXD3 knockout reduced ATPS capacity, ATP content and the mRNA levels of ATPS key subunits with elevated gluconeogenic and lipogenic protein levels in mouse livers (Fig. 8J–M).

4. Discussion

Inhibition of ATP synthesis and increase in ROS production play decisive roles in triggering metabolic disorders [5–7]. ROS are mainly derived from mitochondria, which have multiple ROS producing sites including complex I and complex III in mitochondrial respiratory chain [53,54]. In the process of coupled oxidative phosphorylation, protons are translocated to the intermembrane and generated electrochemical gradient, which is used by ATPS to synthesize ATP. Generally, ATP synthesis process reduces MMP during the leak of protons back to the mitochondrial matrix through ATPS [55]. Administrations of ATPS substrates (ADP and P_i) reduced ROS generation, while treatment with ATPS inhibitors increased ROS production [56]. Meanwhile, reduction in MMP by about 18 % decreased ROS production by about 90 % [56]. However, it should also be noted that not all of ROS production is dependent on MMP [57]. Enzymes from the outer mitochondrial membrane [58], and non-mitochondrial subcellular organelles including peroxisome and endoplasmic reticulum [59] also produce ROS. Cultured fibroblasts of ATP synthase-mutant patients exhibited a decrease in ATP production, high level of MMP after addition of ADP, and an increase in ROS generation [18]. Clearly, reduction of MMP via ATPS-mediated ATP synthesis plays important roles in FAM3A-induced inhibition on ROS production.

Antioxidant system such as SOD also plays important roles in ROS clearance [60]. ROS overproduction, ATP depletion and increased release of inflammatory factors are considered as the main characteristics of ischemia-reperfusion injury (IRI). In our previous study, we observed a decrease in SOD activity in FAM3A-deficient mouse livers with IRI [25]. Activation of FAM3A using rosiglitazone protected the mice against IRI with increased antioxidants such as SOD [25]. In the current study, we further confirmed FAM3A overexpression increased SOD activity in human and mouse hepatocytes, which was supported by one previous study that ATPS inhibitor oligomycin treatment reduced SOD activity [61]. In addition, it had been reported that mild uncoupling of oxidative phosphorylation by mitochondrial uncoupling proteins (UCPs) attenuated ROS production [55]. Six members of UCPs have been identified (UCP1–6) in mammals [62]. UCP1 is uniquely expressed in the brown adipose tissue (BAT) for adaptive thermogenesis [63], while UCP2 is ubiquitously expressed in various tissues [62]. MMP and ROS production were mildly elevated in UCP2-deficient islets [64].

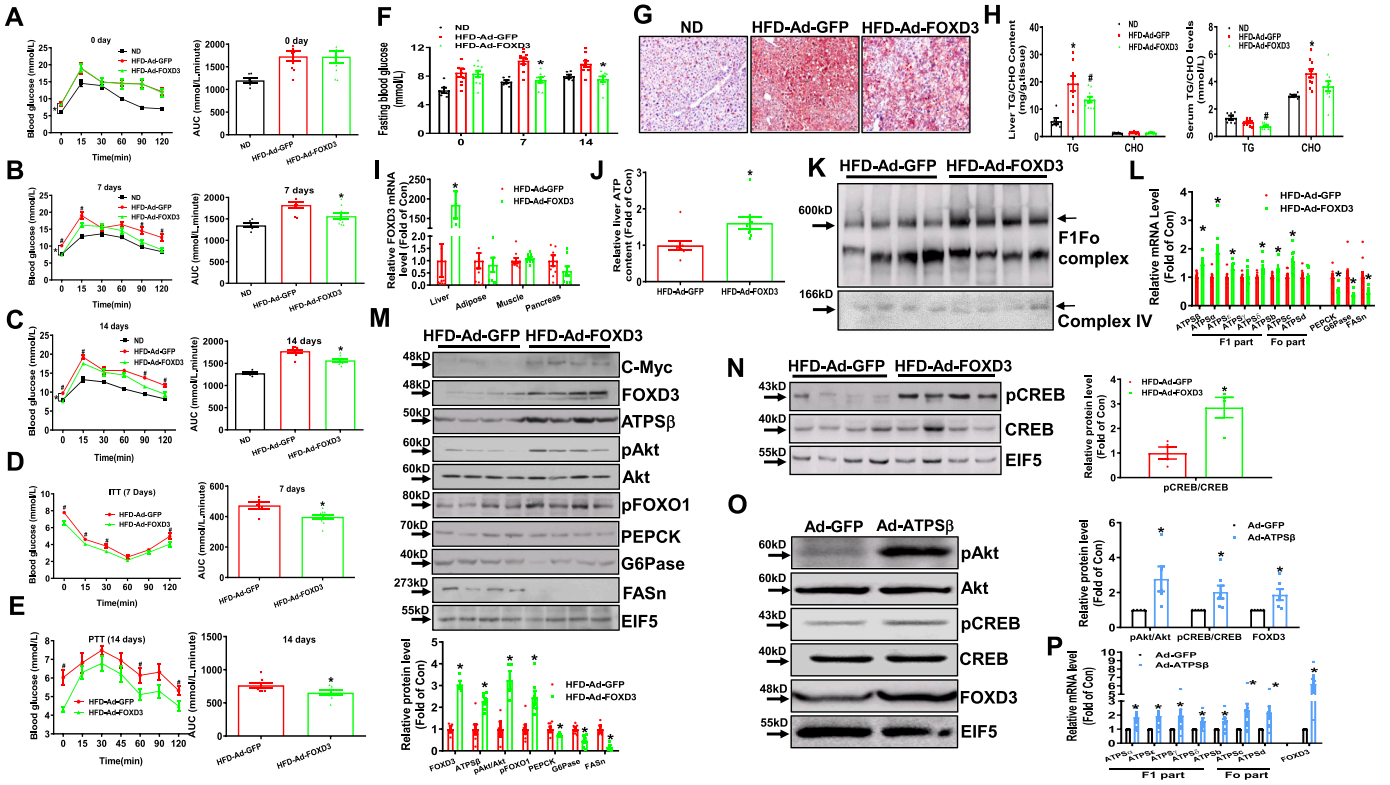

Fig. 6. Hepatic FOXD3 overexpression improved glucose intolerance, insulin resistance, gluconeogenesis and fatty liver in HFD mice. A–C) OGTT at 0, 7 and 14 days post the injection of Ad-FOXD3 or Ad-GFP. The OGTT data were shown in left panel, and area under curve (AUC) data in right panel. D–E) Hepatic overexpression of FOXD3 improved insulin resistance (D) and suppressed hepatic glucose production (E). ITT and PTT were done using one set of mice. ITT was done at 7 days post viral injection, while PTT was done at 14 days post viral injection. Glucose data were shown in left panel, and AUC data in right panel. $^{*}P < 0.05$ ND versus HFD, $^{\#}P < 0.05$ HFD-Ad-GFP versus HFD-Ad-FOXD3. F) Hepatic FOXD3 overexpression ameliorated fasting hyperglycemia of HFD mice. Fasting blood glucose levels were referred to the 0 min data in OGTT shown in panels A–C. N = 8–10, $^{*}P < 0.05$ versus Ad-GFP-treated HFD mice. G–H) FOXD3 overexpression reduced lipid deposition in mouse liver and serum. Representative Oil Red O staining images were shown in panel G, and quantitative analyses of TG and CHO content were shown in panel H. TG, triglycerides; CHO, cholesterol. I) Injection of Ad-FOXD3 influenced the mRNA level of FOXD3 in livers and other tissues of HFD mice. J) FOXD3 overexpression increased ATP content in HFD mouse livers. N = 9. $^{*}P < 0.05$ versus Ad-GFP-treated HFD mice. K) FOXD3 overexpression increased ATPS capacity in HFD mouse livers. Complex IV was assayed as loading control. Complex IV, cytochrome *c* oxidase subunit IV. L) FOXD3 overexpression increased the mRNA levels of key ATPS subunits and decreased the mRNA expression of gluconeogenesis and lipogenesis genes in HFD mice livers. M) FOXD3 overexpression on the protein levels of glucose and lipid metabolic genes in mouse livers. Representative gel images shown in upper panel, and quantitative data in lower panel. N) FOXD3 overexpression on CERB phosphorylation in mouse livers. Representative gel images shown in left panel, and quantitative data in right panel. N = 5–7 for protein analysis, and N = 8–10 for mRNA and ATP assays, $^{*}P < 0.05$ versus Ad-GFP-treated HFD mice. O) ATPSβ overexpression increased CREB phosphorylation and FOXD3 protein level in mouse hepatocytes. Representative gel images shown in left panel, and quantitative data in right panel. P) ATPSβ overexpression increased the mRNA levels of FOXD3 and ATPS subunits in mouse hepatocytes. N = 6, $^{*}P < 0.05$ versus Ad-GFP-infected control cells. (For interpretation of the references to colour in this figure legend, the reader is referred to the web version of this article.)

Similarly, the levels of oxidative stress markers and ROS were increased in UCP2-deficient mouse livers [65]. Our previous study found that FAM3A overexpression or silencing increased or reduced UCP2 expression in mouse livers [24]. Collectively, decreased MMP resulting from ATP synthesis and UCP2 uncoupling, and increased anti-oxidants such as SOD together contributed to the beneficial effects of FAM3A-induced inhibition of ROS generation in hepatocytes. In the current study, we clearly demonstrated that FAM3A is a novel active component of ATPS, and activates ATPS activity by interacting with F1 part to enhance ATP production, accompanied with decreased MMP and ROS production. These new findings greatly expanded the understanding on the biological processes of mitochondrial ATP synthesis and ROS production, and shed light on the pathogenesis of diabetes, NAFLD and other mitochondrial-related diseases.

It has been previously reported that ATP can be released to activate the purinergic P2 receptors, which including P2X and P2Y receptor subtypes, as a signaling molecule in different cell types [66,67]. We had previously established that FAM3A overexpression elevated the intracellular and extracellular ATP content in hepatocytes. FAM3A-promoted ATP release activated P2 receptors to increase cytosolic free calcium level, which activated PI3K-Akt signaling pathway and CPT2 expression in a CaM-dependent manner to suppress gluconeogenesis and increase lipid oxidation in hepatocytes [24,38]. FOXD3 plays critical roles in regulating the formation of neural crest during the early embryo stage, and global knockout of FOXD3 gene causes embryo death in mice [49,68]. FOXD3 is also necessary for stem cells to maintain pluripotency [69–72]. FAM3A interacts with F1-ATPS to increase ATP synthesis and release. Released ATP further activates Akt-CREB to induce FOXD3 expression via P2 receptors in hepatocytes. ATP11 and ATP12 are the ancillary factors that assist the assembly of ATPSβ and ATPSα as F1-ATPS, respectively [73], while TMEM70 determines the efficacy of Fo assembly by controlling the formation of subunit c oligomer in mitochondrial inner membrane [74]. Our findings revealed that FOXD3 universally regulates the transcriptions of F1Fo-ATPS genes, and ancillary factor genes including ATP11, ATP12 and TMEM70 in hepatocytes. As the key catalytic subunit of ATPS, ATPβ overexpression activated ATP generation and promoted ATP release, and then the released ATP activated P2 receptor pathway in hepatocytes [21]. ATPSβ overexpression also induced Akt and CREB phosphorylation to upregulate FOXD3 expression and promote the transcription of other F1Fo-ATPS subunits

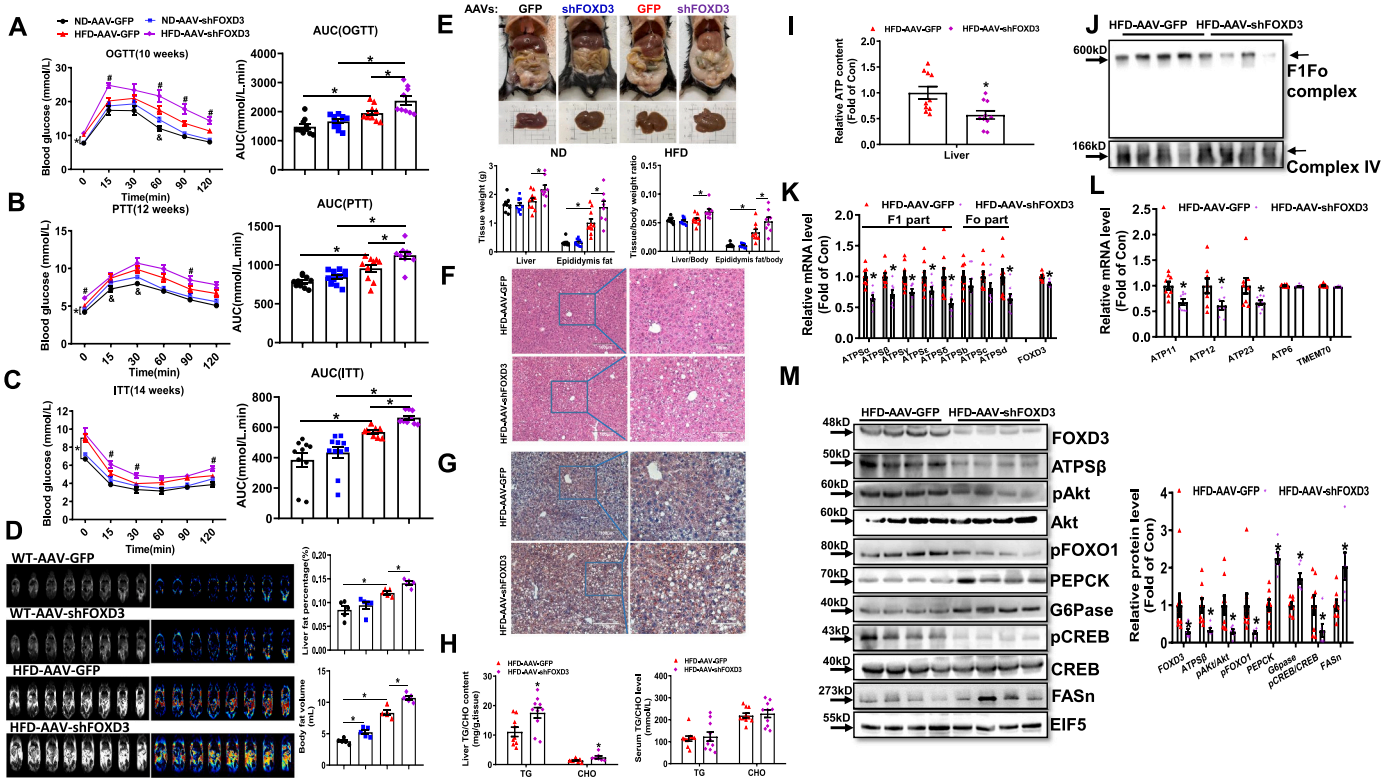

Fig. 7. Hepatic FOXD3 inhibition impaired ATPS assembly and aggravated glucolipid disorders in mice. A–C) OGTT (A), PTT(B) and ITT (C) were performed at 10 weeks, 12 weeks, and 14 weeks, respectively, post AAV-GFP or AAV-shFOXD3 injection. AUC data was shown on the right panel. $^{*}P < 0.05$ ND-AAV-GFP versus HFD-AAV-GFP, $^{\&}P < 0.05$ ND-AAV-GFP versus ND-AAV-shFOXD3, $^{\#}P < 0.05$ HFD-AAV-GFP versus HFD-AAV-shFOXD3. D) MRI analysis of liver and body fat distribution in mice. Representative images were presented in the left panel; quantitative data were shown in the right panel. N = 5, $^{*}P < 0.05$ between indicated groups. E) Morphological analysis of liver and epididymal fat in mice (upper panel), and the liver/fat weight or ratio to body weight were measured and shown on the below. F–G) Representative liver histology by Hematoxylin-Eosin or Oil Red O staining, scale bar = 100 μm. H) Determination of hepatic/serum TG and CHO levels for AAV-GFP or AAV-shFOXD3 mice fed on HFD. I–L) AAV-shFOXD3 injection decreased ATP content (I) and ATPS capacity (J), and reduced the mRNA levels of ATPS key subunits and assembly factors (K–L). M) Protein levels of glucose and lipid metabolic genes after hepatic FOXD3 inhibition. Representative images were shown in left panel, and quantitative data in right panel, respectively. For all figures except (D). N = 9–11, $^{*}P < 0.05$ versus indicated groups. (For interpretation of the references to colour in this figure legend, the reader is referred to the web version of this article.)

and ancillary factors in hepatocytes. These findings revealed a novel regulation loop among ATP, Akt, CREB, FOXD3 and ATPSβ (ATPS), and FAM3A may initiate and control it in hepatocytes (Fig. 8N). This novel regulation loop also provided the direct explanation mechanism for the observation that ATPSβ overexpression alone can effectively enhance mitochondrial ATP production in previous study [21]. What's more, identification of FOXD3 as a general transcription factor that controls ATPS assembly makes it possible and viable to restore ATPS capacity by targeting one single gene under diabetic or other pathophysiological conditions. Particularly, the ATP-CREB-FOXD3-ATPS regulation loop assures that the expressions of ATPS key subunits and ancillary factors can be synchronously stimulated to increase ATPS capacity when ATP need is increased in some conditions such as growth, proliferation and high metabolism. FAM3A-deficiency or inhibition markedly reduced ATP content in liver, muscle, islets, VSMCs and other tissues [29,31–33,75]. Under obese or diabetic condition, FAM3A inhibition by miRNA-423-5p interrupted ATP-CREB-FOXD3-ATPS regulation loop to reduce ATPS capacity and ATP production. Our findings also provided a direct explanation for ATPS capacity and ATP production reduction, and ROS overproduction in livers, islets and other tissues under diabetic or obese condition [8–13,19,21].

It has been widely acknowledged that high MMP not only drives ATP production but also triggers ROS generation [55]. Under obese status, mitochondrial ATP capacity is reduced, and then high MMP resulting from excessive oxidation of glucose and lipid generates excessive ROS to trigger insulin resistance and β cell failure [76–78]. Under obese or diabetic condition, reducing MMP represents an effective strategy for ameliorating oxidative stress. In this circumstance, the beneficial effects of ROS repression may overwhelm the deleterious effects of ATP production. Metformin targets mitochondrial complex I to inhibit electron transfer frequency and reduce MMP, inhibiting both ATP and ROS production [79]. An increase in AMP/ATP or ADP/AMP ratio will activate AMPK to suppress hepatic gluconeogenesis and stimulate glucose uptake [80,81]. It has also been proposed that the reduction of high energy state (high MMP) but not AMPK activation is the main mechanism through which metformin inhibits hepatic gluconeogenesis in mice [82]. Metformin induces a more significant decrease in ATP content in AMPK-deficient mouse livers than in wild type mouse livers [83], suggesting and supporting that AMPK activation is a protective mechanism for maintaining cellular ATP level in case of metformin treatment. Moreover, to reduce MMP using mitochondrial uncouplers such as 2,4-dinitrophenol (DNP) also ameliorated hyperglycemia in obese diabetic mice [84]. However, long-term use of mitochondrial uncouplers may impair the functions of high ATP-consuming tissues such as skeletal muscle and heart [85]. In support, inhibition of uncoupling protein 2 (UCP2) by genipin increases ATP production to improve pancreatic β cell dysfunction under diabetic condition [86]. However, genipin may also increase oxidative stress to impair pancreatic β cell functions [87]. In addition, targeting the enzyme(s)/protein(s) in glycolysis, tricarboxylic acid cycle, mitochondrial complexes I to IV, and UCPs to enhance ATP production by increasing MMP may cause excessive ROS production and oxidative stress. Actually, mice with

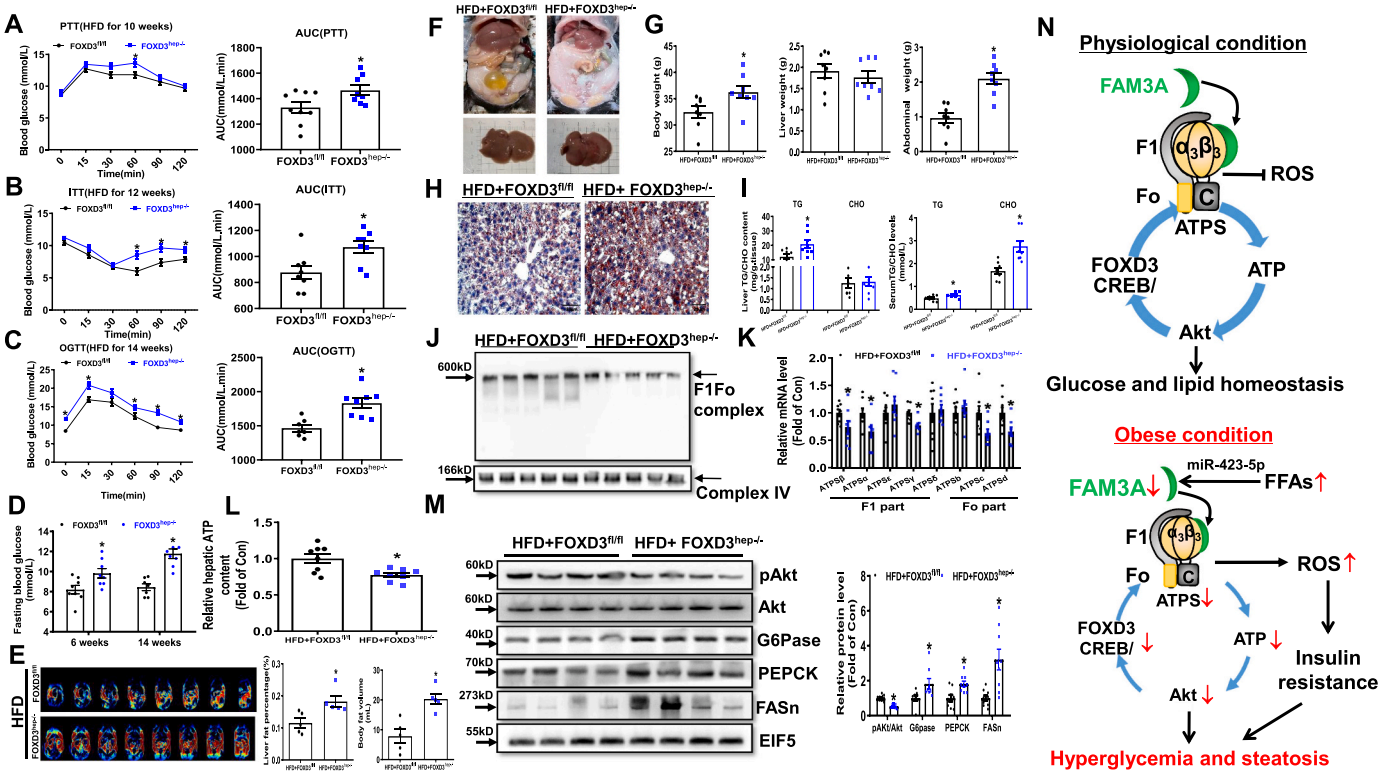

Fig. 8. Hepatic-specific knockout of FOXD3 impaired ATPS assembly and aggravated glucolipid disorders in mice. A–C) PTT (A), ITT (B) and OGTT(C) were performed after fed on HFD 10 weeks, 12 weeks and 14 weeks, respectively. AUC data were shown on the right panel. N = 8. *$P < 0.05$ $FOXD3^{fl/fl}$ versus $FOXD3^{hep-/-}$. D) The fasting glucose levels of mice fed on HFD for 6 weeks and 14 weeks. E) MRI analysis of liver and body fat distribution in mice. Representative images were presented in the left panel, and quantitative data were shown in the right panel. N = 5. F–G) Histomorphology for the mice of indicated groups. Representative images were shown in (F), and quantitative data for body/tissue weight were shown in (G). H) Representative liver histologic images by Oil Red O staining, scale bar = 25 μm. I) Determination of hepatic and serum TG and CHO levels in $FOXD3^{fl/fl}$ and $FOXD3^{hep-/-}$ mice fed on HFD. J–K) ATPS assembly and mRNA levels of ATPS key subunits for indicated groups. N = 8. L) The relative ATP content in livers. N = 8. M) Protein levels of glucose and lipid metabolic genes after hepatic deletion of FOXD3. Representative images were shown in left panel, and quantitative data were show on the right. N = 8. *$P < 0.05$ versus HFD + $FOXD3^{fl/fl}$. N) The proposed mechanism of FAM3A and FOXD3 in regulating mitochondrial ATP production. In physiological condition, FAM3A interacts with F1 part of F1-ATPS to enhance ATP production and release. Released ATP further activates CREB-FOXD3 axis to stimulate the expressions of F1Fo-ATPS complex genes and assembly factor genes, and increase the capacity of ATPS, augmenting ATP production and repressing ROS production. Under obese condition, elevated levels of free fatty acids activate miR-423-5p to inhibit FAM3A expression, interrupt ATP-FOXD3-ATPS regulatory loop to cause mitochondrial dysfunction, resulting in dysregulated glucose and lipid metabolism. Akt, protein kinase B; ATP, adenosine triphosphate; ATPS, ATP Synthase; FAM3A, member A of family with sequence similarity 3; FFAs, free fatty acids; FOXD3, forkhead Box D3; ROS, reactive oxygen species. (For interpretation of the references to colour in this figure legend, the reader is referred to the web version of this article.)

transgenic overexpression of glucokinase in liver exhibited improved glucose tolerance at 3-month old but displayed insulin resistance, glucose intolerance and hyperglycemia at 6-month old [88]. Similarly, glucokinase overexpression increased insulin secretion at low glucose but impaired insulin secretion at high glucose in pancreatic β cells due to oxidative stress [89]. Clearly, the above strategies that aimed to inhibit ROS production were at the risk of impairing mitochondrial ATP production, while that aimed to stimulate ATP synthesis increased ROS production. Although the roles of ROS neutralizing substances, antioxidants, and activation of enzymes of the antioxidant defense system in reducing ROS production should not be ignored, most of them do not affect ATP production. Therefore, to achieve a balance between ROS and ATP production by mitochondria is critical for developing new strategy to treat metabolic disorders. In the current study, we demonstrated that activating FAM3A-FOXD3 axis to restore ATPS assembly represents a promising and viable strategy of enhancing ATP synthesis while reducing ROS production.

In summary, FAM3A is a novel active component of ATPS. FAM3A interacts with F1-ATPS to initially increase ATP production and release, and then the released ATP activates FOXD3 to expand ATPS capacity, augmenting FAM3A's effects on ATP production and ROS inhibition. Under obese condition, FAM3A repression interrupts ATPS-FOXD3 regulation loop to reduce ATPS capacity, triggering mitochondrial dysfunction, and dysregulated glucose and lipid metabolism (Fig. 8N). Activating FAM3A-FOXD3 axis represents a viable strategy for restoring ATPS assembly to treat metabolic disorders.

4.1. *Significance, translational potential and limitation*

The current study had multiple great significances: 1) FAM3A is a new active component of ATPS. 2) FOXD3 is a general transcription factor that controls ATPS assembly, and FAM3A-ATPS-FOXD3 regulation loop plays important roles in controlling ATP synthase assembly and capacity. 3) Identification of FAM3A-FOXD3 axis makes it viable to restore ATPS capacity by activating one single gene under diabetic or other pathophysiological conditions. Activation of FAM3A-FOXD3 axis increases ATPS capacity to restore ATP synthesis and release, and then released ATP activates PI3K-Akt pathway independent of insulin to suppress hepatic gluconeogenesis, which is crucial for treating diabetes, particularly advanced diabetes mainly characterized by severe insulin resistance and pancreatic β cell failure. Moreover, activation of FAM3A-FOXD3 axis also ameliorates oxidative stress, which is one of the key reasons causing insulin resistance and steatosis.

Although FOXD3 and FAM3A overexpression obviously enhanced

ATP production and release to ameliorate glucose and lipid disorders, some potential side effects in other tissues such as VSMCs due to elevated ATP synthesis should be taken into consideration. Drugs or drug delivery systems that specifically target FAM3A expression in liver, pancreatic beta cells and BAT could be further developed for the treatment of metabolic disorders. Moreover, although increased ATP synthesis is beneficial for metabolic diseases, it may also promote the proliferation of cancer cells [90,91]. So, determination of ATP synthesis threshold is important and necessary.

Funding

This study was supported by grants the National Natural Science Foundation of China (82230024/82070844/81870551/82025008), and Beijing Natural Science Foundation (7212123).

CRediT authorship contribution statement

Han Yan: Conceptualization, Methodology, Data curation, Writing – original draft, Writing – review & editing. **Yuhong Meng:** Conceptualization, Methodology, Data curation, Writing – original draft, Writing – review & editing. **Xin Li:** Conceptualization, Methodology, Data curation, Writing – original draft, Writing – review & editing. **Rui Xiang:** Methodology, Data curation. **Song Hou:** Validation, Investigation. **Junpei Wang:** Methodology, Data curation, Resources. **Lin Wang:** Resources. **Xiaoxing Yu:** Methodology, Resources. **Ming Xu:** Supervision, Investigation. **Yujing Chi:** Conceptualization, Supervision, Writing – review & editing, Project administration, Funding acquisition. **Jichun Yang:** Conceptualization, Supervision, Writing – review & editing, Project administration, Funding acquisition.

Declaration of competing interest

The authors declare that there is no conflict of interest.

Data availability

All data are available in the main text or the Supplementary materials.

Appendix A. Supplementary data

Supplementary data to this article can be found online at https://doi.org/10.1016/j.metabol.2022.155372.

References

[1] Sun H, Saeedi P, Karuranga S, Pinkepank M, Ogurtsova K, Duncan BB, et al. IDF diabetes atlas: global, regional and country-level diabetes prevalence estimates for 2021 and projections for 2045. Diabetes Res Clin Pract 2022;183:109119.
[2] Rines AK, Sharabi K, Tavares CD, Puigserver P. Targeting hepatic glucose metabolism in the treatment of type 2 diabetes. Nat Rev Drug Discov 2016;15:786–804.
[3] Zinker B, Mika A, Nguyen P, Wilcox D, Ohman L, von Geldern TW, et al. Liver-selective glucocorticoid receptor antagonism decreases glucose production and increases glucose disposal, ameliorating insulin resistance. Metab Clin Exp 2007;56:380–7.
[4] Anstee QM, Targher G, Day CP. Progression of NAFLD to diabetes mellitus, cardiovascular disease or cirrhosis. Nat Rev Gastroenterol Hepatol 2013;10:330–44.
[5] Koliaki C, Roden M. Alterations of mitochondrial function and insulin sensitivity in human obesity and diabetes mellitus. Annu Rev Nutr 2016;36:337–67.
[6] Pinti MV, Fink GK, Hathaway QA, Durr AJ, Kunovac A, Hollander JM. Mitochondrial dysfunction in type 2 diabetes mellitus: an organ-based analysis. Am J Physiol Endocrinol Metab 2019;316:E268–85.
[7] Yaribeygi H, Atkin SL, Sahebkar A. Mitochondrial dysfunction in diabetes and the regulatory roles of antidiabetic agents on the mitochondrial function. J Cell Physiol 2019;234:8402–10.
[8] Miyamoto A, Takeshita M, Pan-Hou H, Fujimori H. Hepatic changes in adenine nucleotide levels and adenosine 3'-monophosphate forming enzyme in streptozotocin-induced diabetic mice. J Toxicol Sci 2008;33:209–17.
[9] Berglund ED, Lee-Young RS, Lustig DG, Lynes SE, Donahue EP, Camacho RC, et al. Hepatic energy state is regulated by glucagon receptor signaling in mice. J Clin Invest 2009;119:2412–22.
[10] Serviddio G, Bellanti F, Tamborra R, Rollo T, Romano AD, Giudetti AM, et al. Alterations of hepatic ATP homeostasis and respiratory chain during development of non-alcoholic steatohepatitis in a rodent model. Eur J Clin Invest 2008;38:245–52.
[11] Szendroedi J, Chmelik M, Schmid AI, Nowotny P, Brehm A, Krssak M, et al. Abnormal hepatic energy homeostasis in type 2 diabetes. Hepatology 2009;50:1079–86.
[12] Schmid AI, Szendroedi J, Chmelik M, Krssak M, Moser E, Roden M. Liver ATP synthesis is lower and relates to insulin sensitivity in patients with type 2 diabetes. Diabetes Care 2011;34:448–53.
[13] Sharma R, Sinha S, Danishad KA, Vikram NK, Gupta A, Ahuja V, et al. Investigation of hepatic gluconeogenesis pathway in non-diabetic asian indians with non-alcoholic fatty liver disease using in vivo ((31)P) phosphorus magnetic resonance spectroscopy. Atherosclerosis 2009;203:291–7.
[14] Martinez-Reyes I, Chandel NS. Mitochondrial TCA cycle metabolites control physiology and disease. Nat Commun 2020;11:102.
[15] Cingolani G, Duncan TM. Structure of the ATP synthase catalytic complex (F(1)) from Escherichia coli in an autoinhibited conformation. Nat Struct Mol Biol 2011;18:701–7.
[16] Sabbert D, Engelbrecht S, Junge W. Intersubunit rotation in active F-ATPase. Nature 1996;381:623–5.
[17] Hahn A, Vonck J, Mills DJ, Meier T, Kuhlbrandt W. Structure, mechanism, and regulation of the chloroplast ATP synthase. Science 2018;360.
[18] Mracek T, Pecina P, Vojtiskova A, Kalous M, Sebesta O, Houstek J. Two components in pathogenic mechanism of mitochondrial ATPase deficiency: energy deprivation and ROS production. Exp Gerontol 2006;41:683–7.
[19] Vendemiale G, Grattagliano I, Caraceni P, Caraccio G, Domenicali M, Dall'Agata M, et al. Mitochondrial oxidative injury and energy metabolism alteration in rat fatty liver: effect of the nutritional status. Hepatology 2001;33:808–15.
[20] Echeverria F, Valenzuela R, Bustamante A, Alvarez D, Ortiz M, Espinosa A, et al. High-fat diet induces mouse liver steatosis with a concomitant decline in energy metabolism: attenuation by eicosapentaenoic acid (EPA) or hydroxytyrosol (HT) supplementation and the additive effects upon EPA and HT co-administration. Food Funct 2019;10:6170–83.
[21] Wang C, Chen Z, Li S, Zhang Y, Jia S, Li J, et al. Hepatic overexpression of ATP synthase beta subunit activates PI3K/Akt pathway to ameliorate hyperglycemia of diabetic mice. Diabetes 2014;63:947–59.
[22] Walker JE. The ATP synthase: the understood, the uncertain and the unknown. Biochem Soc Trans 2013;41:1–16.
[23] Zhu Y, Xu G, Patel A, McLaughlin MM, Silverman C, Knecht K, et al. Cloning, expression, and initial characterization of a novel cytokine-like gene family. Genomics 2002;80:144–50.
[24] Wang C, Chi Y, Li J, Miao Y, Li S, Su W, et al. FAM3A activates PI3K p110alpha/Akt signaling to ameliorate hepatic gluconeogenesis and lipogenesis. Hepatology 2014;59:1779–90.
[25] Chen Z, Wang J, Yang W, Chen J, Meng Y, Geng B, et al. FAM3A mediates PPARgamma's protection in liver ischemia-reperfusion injury by activating akt survival pathway and repressing inflammation and oxidative stress. Oncotarget 2017;8:49882–96.
[26] Zhang X, Yang W, Wang J, Meng Y, Guan Y, Yang J. FAM3 gene family: a promising therapeutical target for NAFLD and type 2 diabetes. Metab Clin Exp 2018;81:71–82.
[27] Chen Z, Liu X, Luo Y, Wang J, Meng Y, Sun L, et al. Repurposing doxepin to ameliorate steatosis and hyperglycemia by activating FAM3A signaling pathway. Diabetes 2020;69:1126–39.
[28] Zhang Y, Wan J, Liu S, Hua T, Sun Q. Exercise induced improvements in insulin sensitivity are concurrent with reduced NFE2/miR-432-5p and increased FAM3A. Life Sci 2018;207:23–9.
[29] Chi Y, Li J, Li N, Chen Z, Ma L, Peng W, et al. FAM3A enhances adipogenesis of 3T3-L1 preadipocytes via activation of ATP-P2 receptor-akt signaling pathway. Oncotarget 2017;8:45862–73.
[30] Jia S, Chen Z, Li J, Chi Y, Wang J, Li S, et al. FAM3A promotes vascular smooth muscle cell proliferation and migration and exacerbates neointima formation in rat artery after balloon injury. J Mol Cell Cardiol 2014;74:173–82.
[31] Xiang R, Chen J, Li S, Yan H, Meng Y, Cai J, et al. VSMC-specific deletion of FAM3A attenuated ang II-promoted hypertension and cardiovascular hypertrophy. Circ Res 2020;126:1746–59.
[32] Yang W, Chi Y, Meng Y, Chen Z, Xiang R, Yan H, et al. FAM3A plays crucial roles in controlling PDX1 and insulin expressions in pancreatic beta cells. FASEB J 2020;34:3915–31.
[33] Yan H, Chen Z, Zhang H, Yang W, Liu X, Meng Y, et al. Intracellular ATP signaling contributes to FAM3A-induced PDX1 upregulation in pancreatic Beta cells. Exp Clin Endocrinol Diabetes 2022;130(8):498–508.
[34] Zhou Y, Jia S, Wang C, Chen Z, Chi Y, Li J, et al. FAM3A is a target gene of peroxisome proliferator-activated receptor gamma. Biochim Biophys Acta 2013;1830:4160–70.
[35] Song Q, Gou WL, Zhang R. FAM3A protects HT22 cells against hydrogen peroxide-induced oxidative stress through activation of PI3K/Akt but not MEK/ERK pathway. Cell Physiol Biochem 2015;37:1431–41.
[36] Song Q, Gou WL, Zhang R. FAM3A attenuates ER stress-induced mitochondrial dysfunction and apoptosis via CHOP-wnt pathway. Neurochem Int 2016;94:82–9.

[37] Liu J, An P, Xue Y, Che D, Liu X, Zheng J, et al. Mechanism of Snhg8/miR-384/Hoxa13/FAM3A axis regulating neuronal apoptosis in ischemic mice model. Cell Death Dis 2019;10:441.
[38] Liu X, Hou S, Xiang R, Hu C, Chen Z, Li N, et al. Imipramine activates FAM3A-FOXA2-CPT2 pathway to ameliorate hepatic steatosis. Metab Clin Exp 2022;136:155292.
[39] Nishimura N, Gotoh T, Oike Y, Yano M. TMEM65 is a mitochondrial inner-membrane protein. PeerJ. 2014;2:e349.
[40] Cizkova A, Stranecky V, Mayr JA, Tesarova M, Havlickova V, Paul J, et al. TMEM70 mutations cause isolated ATP synthase deficiency and neonatal mitochondrial encephalocardiomyopathy. Nat Genet 2008;40:1288–90.
[41] Eruslanov E, Kusmartsev S. Identification of ROS using oxidized DCFDA and flow-cytometry. Methods Mol Biol (Clifton, NJ) 2010;594:57–72.
[42] Sukumar M, Liu J, Mehta GU, Patel SJ, Roychoudhuri R, Crompton JG, et al. Mitochondrial membrane potential identifies cells with enhanced stemness for cellular therapy. Cell Metab 2016;23:63–76.
[43] Du L, Lin L, Li Q, Liu K, Huang Y, Wang X, et al. IGF-2 preprograms maturing macrophages to acquire oxidative phosphorylation-dependent anti-inflammatory properties. Cell Metab 2019;29(1363–75):e8.
[44] Zhang T, Wang Y, Kang Y, Wang L, Zhao H, Ji X, et al. Testosterone enhances mitochondrial complex V function in the substantia nigra of aged male rats. Aging 2020;12:10398–414.
[45] Yang Y, Li J, Wei C, He Y, Cao Y, Zhang Y, et al. Amelioration of nonalcoholic fatty liver disease by swertiamarin in fructose-fed mice. Phytomedicine 2019;59:152782.
[46] Wang J, Yang W, Chen Z, Chen J, Meng Y, Feng B, et al. Long noncoding RNA lncSHGL recruits hnRNPA1 to suppress hepatic gluconeogenesis and lipogenesis. Diabetes 2018;67:581–93.
[47] Chen Z, Wang J, Yang W, Chen J, Meng Y, Feng B, et al. FAM3C activates HSF1 to suppress hepatic gluconeogenesis and attenuate hyperglycemia of type 1 diabetic mice. Oncotarget 2017;8:106038–49.
[48] Zheng ZG, Zhang X, Liu XX, Jin XX, Dai L, Cheng HM, et al. Inhibition of HSP90beta improves lipid disorders by promoting mature SREBPs degradation via the ubiquitin-proteasome system. Theranostics 2019;9:5769–83.
[49] Hanna LA, Foreman RK, Tarasenko IA, Kessler DS, Labosky PA. Requirement for Foxd3 in maintaining pluripotent cells of the early mouse embryo. Genes Dev 2002;16:2650–61.
[50] Plank JL, Frist AY, LeGrone AW, Magnuson MA, Labosky PA. Loss of Foxd3 results in decreased beta-cell proliferation and glucose intolerance during pregnancy. Endocrinology 2011;152:4589–600.
[51] Shahrestanaki MK, Arasi FP, Aghaei M. IPP-1 controls Akt/CREB phosphorylation extension in A2a adenosine receptor signaling cascade in MIN6 pancreatic beta-cell line. Eur J Pharmacol 2019;850:88–96.
[52] Xiang Q, Zhang J, Li CY, Wang Y, Zeng MJ, Cai ZX, et al. Insulin resistance-induced hyperglycemia decreased the activation of Akt/CREB in hippocampus neurons: molecular evidence for mechanism of diabetes-induced cognitive dysfunction. Neuropeptides 2015;54:9–15.
[53] Murphy MP. How mitochondria produce reactive oxygen species. Biochem J 2009;417:1–13.
[54] Yao L, Liang X, Qiao Y, Chen B, Wang P, Liu Z. Mitochondrial dysfunction in diabetic tubulopathy. Metab Clin Exp 2022;131:155195.
[55] Cadenas S. Mitochondrial uncoupling, ROS generation and cardioprotection. Biochim Biophys Acta Bioenerg 2018;1859:940–50.
[56] Korshunov SS, Skulachev VP, Starkov AA. High protonic potential actuates a mechanism of production of reactive oxygen species in mitochondria. FEBS Lett 1997;416:15–8.
[57] Lambert AJ, Brand MD. Superoxide production by NADH:ubiquinone oxidoreductase (complex I) depends on the pH gradient across the mitochondrial inner membrane. Biochem J 2004;382:511–7.
[58] Andreyev AY, Kushnareva YE, Starkov AA. Mitochondrial metabolism of reactive oxygen species. Biochem Biokhim 2005;70:200–14.
[59] Forrester SJ, Kikuchi DS, Hernandes MS, Xu Q, Griendling KK. Reactive oxygen species in metabolic and inflammatory signaling. Circ Res 2018;122:877–902.
[60] Roberts CK, Barnard RJ, Sindhu RK, Jurczak M, Ehdaie A, Vaziri ND. Oxidative stress and dysregulation of NAD(P)H oxidase and antioxidant enzymes in diet-induced metabolic syndrome. Metab Clin Exp 2006;55:928–34.
[61] Afolayan AJ, Teng RJ, Eis A, Rana U, Broniowska KA, Corbett JA, et al. Inducible HSP70 regulates superoxide dismutase-2 and mitochondrial oxidative stress in the endothelial cells from developing lungs. Am J Physiol Lung Cell Mol Physiol 2014;306:L351–60.
[62] Monteiro BS, Freire-Brito L, Carrageta DF, Oliveira PF, Alves MG. Mitochondrial uncoupling proteins (UCPs) as key modulators of ROS homeostasis: a crosstalk between diabesity and male Infertility? Antioxidants 2021:10.
[63] Okamatsu-Ogura Y, Kuroda M, Tsutsumi R, Tsubota A, Saito M, Kimura K, et al. UCP1-dependent and UCP1-independent metabolic changes induced by acute cold exposure in brown adipose tissue of mice. Metab Clin Exp 2020;113:154396.
[64] Robson-Doucette CA, Sultan S, Allister EM, Wikstrom JD, Koshkin V, Bhattacharjee A, et al. Beta-cell uncoupling protein 2 regulates reactive oxygen species production, which influences both insulin and glucagon secretion. Diabetes 2011;60:2710–9.
[65] Horimoto M, Fulop P, Derdak Z, Wands JR, Baffy G. Uncoupling protein-2 deficiency promotes oxidant stress and delays liver regeneration in mice. Hepatology 2004;39:386–92.
[66] Burnstock G. Purinergic signaling in the cardiovascular system. Circ Res 2017;120:207–28.
[67] Li J, Yan H, Xiang R, Yang W, Ye J, Yin R, et al. ATP secretion and metabolism in regulating pancreatic Beta cell functions and hepatic glycolipid metabolism. Front Physiol 2022;13:918042.
[68] Fairchild CL, Conway JP, Schiffmacher AT, Taneyhill LA, Gammill LS. FoxD3 regulates cranial neural crest EMT via downregulation of tetraspanin18 independent of its functions during neural crest formation. Mech Dev 2014;132:1–12.
[69] Drerup CM, Wiora HM, Topczewski J, Morris JA. Disc1 regulates foxd3 and sox10 expression, affecting neural crest migration and differentiation. Development 2009;136:2623–32.
[70] Krishnakumar R, Chen AF, Pantovich MG, Danial M, Parchem RJ, Labosky PA, et al. FOXD3 regulates pluripotent stem cell potential by simultaneously initiating and repressing enhancer activity. Cell Stem Cell 2018;23:306–7.
[71] Yong JS, Intriago-Baldeon DP, Lam EW. FOXD3 controls pluripotency through modulating enhancer activity. Stem Cell Investig 2016;3:17.
[72] Arduini BL, Brivanlou AH. Modulation of FOXD3 activity in human embryonic stem cells directs pluripotency and paraxial mesoderm fates. Stem Cells 2012;30:2188–98.
[73] Ackerman SH. Atp11p and Atp12p are chaperones for F(1)-ATPase biogenesis in mitochondria. Biochim Biophys Acta 2002;1555:101–5.
[74] Kovalcikova J, Vrbacky M, Pecina P, Tauchmannova K, Nuskova H, Kaplanova V, et al. TMEM70 facilitates biogenesis of mammalian ATP synthase by promoting subunit c incorporation into the rotor structure of the enzyme. FASEB J 2019;33:14103–17.
[75] Yang W, Wang J, Chen Z, Chen J, Meng Y, Chen L, et al. NFE2 induces miR-423-5p to promote gluconeogenesis and hyperglycemia by repressing the hepatic FAM3A-ATP-akt pathway. Diabetes 2017;66:1819–32.
[76] Zorov DB, Juhaszova M, Sollott SJ. Mitochondrial reactive oxygen species (ROS) and ROS-induced ROS release. Physiol Rev 2014;94:909–50.
[77] Samuel VT, Petersen KF, Shulman GI. Lipid-induced insulin resistance: unravelling the mechanism. Lancet 2010;375:2267–77.
[78] Eguchi N, Vaziri ND, Dafoe DC, Ichii H. The role of oxidative stress in pancreatic beta cell dysfunction in diabetes. Int J Mol Sci 2021;22.
[79] Pernicova I, Korbonits M. Metformin–mode of action and clinical implications for diabetes and cancer. Nat Rev Endocrinol 2014;10:143–56.
[80] Viollet B, Guigas B, Leclerc J, Hebrard S, Lantier L, Mounier R, et al. AMP-activated protein kinase in the regulation of hepatic energy metabolism: from physiology to therapeutic perspectives. Acta Physiol (Oxf) 2009;196:81–98.
[81] Zhang CS, Li M, Wang Y, Li X, Zong Y, Long S, et al. The aldolase inhibitor aldometanib mimics glucose starvation to activate lysosomal AMPK. Nat Metab 2022;4:1369–401.
[82] Foretz M, Hebrard S, Leclerc J, Zarrinpashneh E, Soty M, Mithieux G, et al. Metformin inhibits hepatic gluconeogenesis in mice independently of the LKB1/AMPK pathway via a decrease in hepatic energy state. J Clin Invest 2010;120:2355–69.
[83] Viollet B, Athea Y, Mounier R, Guigas B, Zarrinpashneh E, Horman S, et al. AMPK: lessons from transgenic and knockout animals. Front Biosci (Landmark Ed) 2009;14:19–44.
[84] Perry RJ, Kim T, Zhang XM, Lee HY, Pesta D, Popov VB, et al. Reversal of hypertriglyceridemia, fatty liver disease, and insulin resistance by a liver-targeted mitochondrial uncoupler. Cell Metab 2013;18:740–8.
[85] Demine S, Renard P, Arnould T. Mitochondrial uncoupling: a key controller of biological processes in physiology and diseases. Cells 2019:8.
[86] Zhang CY, Parton LE, Ye CP, Krauss S, Shen R, Lin CT, et al. Genipin inhibits UCP2-mediated proton leak and acutely reverses obesity- and high glucose-induced beta cell dysfunction in isolated pancreatic islets. Cell Metab 2006;3:417–27.
[87] Liu L, Liu J, Gao Y, Yu X, Xu G, Huang Y. Uncoupling protein-2 mediates the protective action of berberine against oxidative stress in rat insulinoma INS-1E cells and in diabetic mouse islets. Br J Pharmacol 2014;171:3246–54.
[88] Ferre T, Riu E, Franckhauser S, Agudo J, Bosch F. Long-term overexpression of glucokinase in the liver of transgenic mice leads to insulin resistance. Diabetologia 2003;46:1662–8.
[89] Wang H, Iynedjian PB. Modulation of glucose responsiveness of insulinoma beta-cells by graded overexpression of glucokinase. Proceedings of the National Academy of Sciences of the United States of America 1997;94:4372–7.
[90] Ge Q, Jia D, Cen D, Qi Y, Shi C, Li J, et al. Micropeptide ASAP encoded by LINC00467 promotes colorectal cancer progression by directly modulating ATP synthase activity. J Clin Invest 2021;131.
[91] Yegutkin GG, Boison D. ATP and adenosine metabolism in cancer: exploitation for therapeutic gain. Pharmacol Rev 2022;74:797–822.